INVESTIGATION OF CALIBRATION-FREE RESOLUTION TECHNIQUES AND INDEPENDENT COMPONENT ANALYSIS

S.Triadaphillou, I.Wells*, A. J. Morris and E. B. Martin

Centre for Process Analytics and Control Technology,,
School of Chemical Engineering and Advanced Materials,
University of Newcastle, Newcastle upon Tyne, NE1 7RU, UK
**Avecia, Process Technology Department, Grangemouth, FK3 8XG, UK*

Abstract: Calibration-free resolution techniques provide an alternative approach to the development of a calibration model. These combine spectroscopic measurement coupled with mathematical and statistical assumptions and give spectral profiles and non-quantitative concentration profiles for the unknown mixture. In this paper, a number of calibration free techniques including VARIMAX, ITTFA, EFA, FSWEFA, SIMPLISMA are described and applied to a synthetic spectral data set and the results are compared with the complementary technique of Independent Component Analysis (ICA) in particular FastICA and JADE. The results were comparable in all cases with ICA separating the signal from the constituent components successfully.

Keywords: Reaction Monitoring and Control, Spectral Conjunction, Spectral Deconvolution, Multivariate Calibration, Iterative Resolution Methods

1. INTRODUCTION

A number of issues are associated with the development of calibration models to predict the concentration of a product in a reaction. For example their development in terms of data generation and collection can be time consuming, the model will be sensitive to changes in process conditions and it only provides quantitative information about the property of interest with no information about side reactions and intermediates. An alternative approach is the family of calibration free resolution techniques. These enable the analyst to make full use of time resolved spectra for the determination of both qualitative and quantitative information, i.e. pure spectra and concentration profiles over the course of a reaction. In addition, on-line analysis of laboratory reactions can markedly improve both the timeliness and quality of information regarding mechanisms and kinetics, compared to the more traditional approaches of extractive sampling. Thus the application of calibration-free methods for on-line analysis can result in major advantages in terms of the understanding of a process.

Most calibration-free resolution techniques are based on the assumption that the instrumental response in a mixture is an additive linear combination of the signals from individual species, the pure components. Consequently it obeys Beer's law, i.e. the spectral response of the components is independent of time and concentration (Miller and Steele, 1990). In the case of reaction monitoring, the spectroscopic response, $\mathbf{R}$ ($I \times J$) is a function of time, t, and spectral wavelength, l. A mixture of K components gives a response, $\mathbf{R}$:

$$r_{i,j}(t,l) = \sum_{k=1}^{K} \mathbf{c}_k(t)\mathbf{s}_k(l) \tag{1}$$

where $\mathbf{c}_k(t)$ is the concentration of component k at time, t, and $\mathbf{s}_k(l)$ is the spectral response of component, k, for wavelength, l.

In this paper, a number of calibration free techniques are investigated including VARIMAX, ITTFA, EFA, FSWEFA and SIMPLISMA. These are compared with Independent Component Analysis (ICA). ICA performs a similar function to the calibration free techniques. It is a separation method that has been applied in speech, biomedical signal processing, financial time series, wireless communications and image feature extraction.

2. SYNTHETIC DATA SET

A synthetic data set was generated from an isothermal batch reaction:

$$A \xrightarrow{k_1} B \xrightarrow{k_2} C$$

where the reaction rates take the values, k_1=0.8, k_2=0.8. The reaction is defined by the following kinetic equations:

$$[A]_t = [A]_0 \exp(-k_1 t) \tag{2}$$

$$[B]_t = \frac{[A]_0 k_1}{k_2 - k_1}(\exp(-k_1 t) - \exp(-k_2 t)) \tag{3}$$

$$[C]_t = [A]_0 - [A]_t - [B]_t \tag{4}$$

where $[A]_0$ is the initial concentration of A, and $[A]_t$, $[B]_t$ and $[C]_t$ are the concentrations of A, B and C, respectively at time t.

Calibration free techniques offer a methodology to monitor a reaction to determine the kinetic profiles of A, B and C. In the case where the components A, B and C are unknown, calibration free techniques can help identify the spectral profiles. To resolve the data set, the following techniques a) PCA (PLS Toolbox) b) EFA (PLS Toolbox) c) EFA (Tauler's Toolbox) d)FW-EFA (Tauler's Toolbox) e) SIMPLISMA f) ITTFA were investigated.

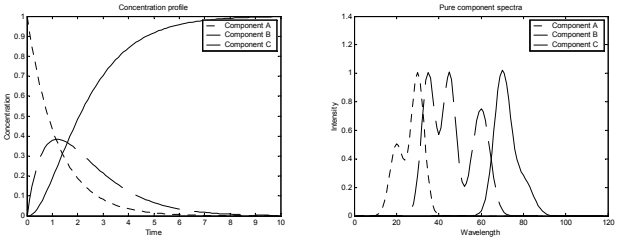

Fig. 1. Concentration profiles of A, B and C as defined by equations 2, 3 and 4.

Fig. 1 shows the concentration profiles and the pure spectra profiles for the three components of the reaction. It can be concluded that the concentration of component A, a reagent, reduces over time, while the concentration of B, an intermediate, increases and then slowly decreases and the concentration of component C, the final product increases with time. From the spectral profile, it can be observed that component A has two peaks at the 20th and 30th wavelength. Component B has three peaks at the 40th, 50th and 60th wavelength and component C has only one peak at the 70th wavelength. The concentration and pure component spectra profiles can be combined to produce a response matrix, **R**, equation 5 that defines absorbances for various wavelengths Fig. 2. This matrix is then used to reproduce the concentration and spectral profiles.

$$\mathbf{R} = \mathbf{C}^T \cdot \mathbf{S} \tag{5}$$

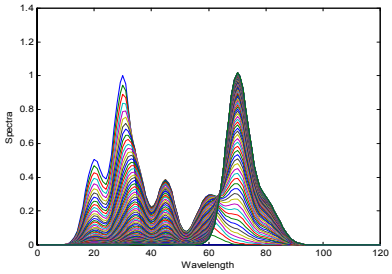

Fig. 2. Graphical representation of matrix **R**.

3. PRINCIPAL COMPONENT ANALYSIS

If the number of components in a reaction is unknown, a first estimate can be obtained through the application of Principal Component Analysis (PCA). A data matrix representing I observations on J variables can be decomposed into two matrices:

$$\mathbf{R} = \mathbf{T} \cdot \mathbf{W}^T \tag{6}$$

where **R** is the spectroscopic response, $(I \times J)$, **W** is the loadings matrix, ($J \times N$) and **T** is the scores matrix, ($I \times N$). For the specific reaction being considered, three components were selected from the application of PCA since the eigenvalue of the third component was still in excess of unity. This is in accord with the expected result.

4. EVOLVING FACTOR ANALYSIS

Evolving Factor Analysis (EFA) is based on the concept of sequential expanding windows, Keller and Massart (1992). A series of spectra from a reaction mixture, which contains a number of different absorbing species, are measured. As the order of the spectra in a chemical reaction provides

additional information, sub-matrices are formed by adding rows to an initial sub-matrix. By analysing the ranks of the data matrices as a function of the number of additional rows, time windows are derived. The number of species involved is equal to the number of significant eigenvalues of the second moment matrix. As new absorbing species start to become significant, new factors/eigenvalues evolve which explain the variability in the process.

EFA makes use of information in the time domain that for other approaches is ignored. In a reaction, the compound that appears first in the spectra should also be the first to disappear. Based on this concept, Tauler and Barcelo (1993) developed a technique to reconstruct the concentration profiles in reactions. For this technique, the compound windows are found by connecting the line of the compound that first appeared with the line of the last compound that appeared, both lines are then combined in a single figure from which the concentration windows are reconstructed. These profiles of the eigenvalues can be considered as a first estimate of the concentration profiles. EFA was applied to the synthetic data set, Fig. 3.

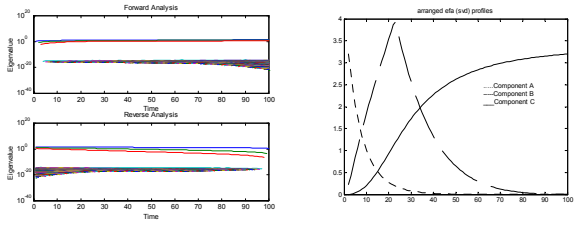

(a) PLS Toolbox (b) Tauler's Toolbox

Fig 3. Results from application of EFA.

From the results of the application of the algorithm from the PLS Toolbox, it can be observed that the forward analysis indicates that 3 independent factors have evolved. One factor appears at the onset of the reaction, a second soon after the first and a third after the second. It is clear that these three factors correspond to the reagent, the intermediate and the final product. The backward analysis suggests that there is only one factor remaining at the end of the reaction with the two other factors disappearing. Once again the results confirm what is known about the reaction.

Application of EFA using the approach in Tauler's Toolbox, which involves a combined analysis of the data matrix, provides an initial estimate of the concentration profiles. However for this data set the concentration profile of the intermediate appears to have shifted from the baseline and the concentration at time point 22 is larger than expected.

5. FIXED WINDOW EVOLVING FACTOR ANALYSIS

A method that is similar to EFA is that of Fixed-Size Window Evolving Analysis (FSWEFA), Cuesta Sanchez *et al*, (1997). In FSWEFA the idea of the fixed-size window is introduced. A small 'window' of rows is selected that is moved over the data set. Analogous to the EFA plots, the eigenvalues of the fixed window (or their log) is plotted against analysis time. In some situations, it is possible to calculate the singular value decomposition at each window position and the associated values are plotted as a function of the window position. The main advantage of FWEFA over EFA is that it is able to detect low concentrations of impurities even at low separations. This is the situation in this example where the second eigenvalue corresponds to the impurity and the impurity under the main component can be localised.

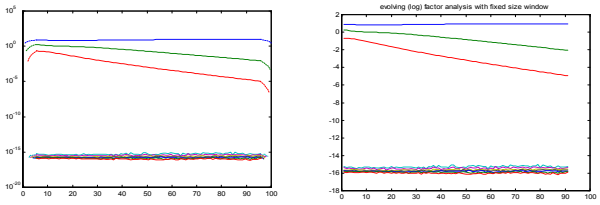

(a) PLS Toolbox (b) Tauler's Toolbox

Fig. 4. Results from application of FSWEFA.

For the fixed window method both the approach described in the PLS Toolbox and Tauler's Toolbox were used with a fixed window size of 10 (Tauler, 2002). As can be seen from Fig. 4, both approaches give similar results, i.e. both identify three factors.

6. SIMPLISMA – PURE VARIABLES

SIMPLISMA is a method that identifies pure variables (Vandeginste *et al*, 2002; Gourvenec *et al*, 2002). It is based on the evaluation of the relative standard deviation of each column of data matrix, **R**. The idea is that a large relative standard deviation is indicative of high purity. Once the pure variables have been identified, the data set can be resolved into the pure spectra. The iterative algorithm for pure variables, for the SIMPLISMA method is as follows. Suppose that the inverse of the data matrix is represented by **D**, ($J \times I$) with elements $d_{j,i}$, where J is the number of variables and I is the number of spectra. First the length λ_j for variable j is calculated:

$$\lambda_j = \left(\left(\frac{1}{I} \right) \sum_{i=1}^{I} (d_{j,i})^2 \right)^{\frac{1}{2}} \qquad (7)$$

where $\lambda_j^2 = \mu_j^2 + \sigma_j^2$, μ_j is the mean of variable j, and σ_j is the standard deviation of variable j. The next step is the calculation of the first relative standard deviation (first purity) for variable j, $p_{j,1}$:

$$p_{j,1} = \frac{\sigma_j}{\mu_j} \tag{8}$$

For variables with low noise range intensity, problems can arise. This occurs because the value of μ_j approaches zero so the value of $p_{j,1}$ will be large. To address this, the purity and length are re-defined and a noise correction term is added. The next pure variable is then determined as the one most independent of the first pure variable. The data matrix is scaled by its length:

$$\delta_{j,i} = \frac{d_{j,i}}{\lambda_j} = \frac{d_{j,i}}{(\mu_j^2 + (\sigma_j + a)^2)^{1/2}} \tag{9}$$

where a is the correction factor for low intensity variables. The correlation about the origin matrix, $\mathbf{\Gamma}$ is defined as follows:

$$\mathbf{\Gamma} = \left(1/I\right)(\lambda)\mathbf{D}(\lambda)^T \tag{10}$$

and the determinant is calculated for variable i

$$\omega_{j,2} = \begin{vmatrix} \gamma_{j,j} & \gamma_{j,p_1} \\ \gamma_{p_1,j} & \gamma_{p_1,p_1} \end{vmatrix} \tag{11}$$

where the index p_1 represents the index for the first pure variable. The determinant is used as a weighting function and as a consequence the elements of the second purity spectrum become:

$$p_{i,2} = (\sigma_i / (\mu_i + a)) \cdot \omega_{i,2} \tag{12}$$

and the equation for the standard deviation spectrum is given by:

$$\sigma_{j,i}^s = \sigma_j \omega_{j,i} \tag{13}$$

For the general case, where j>2 the determinant is:

$$\omega_{j,i} = \begin{vmatrix} \gamma_{j,j} & \gamma_{j,p_1} & \cdots & \gamma_{j,pi-1} \\ \gamma_{p_1,j} & \gamma_{p_1,p_1} & \cdots & \gamma_{p_1,p_{i-1}} \\ \cdots & \cdots & \cdots & \cdots \\ \gamma_{p_{i-1},j} & \cdots & \cdots & \gamma_{p_{i-1},p_{i-1}} \end{vmatrix} \tag{14}$$

and in a similar manner to equation (8), the general formulation for the purity spectrum is $p_{j,i} = (\sigma_j / (\mu_j + a)) \cdot \omega_{j,i}$ and with the correction factor a included, the values for $\omega_{j,1}$ become:

$$\omega_{j,1} = \lambda_j^2 / (\mu_j^2 + (\sigma_j + a)^2) \tag{15}$$

For the identification of pure variables, the number of components was set to three and the noise allowed was 5%. The results can be seen in Fig. 5. The final profiles in Fig. 5 can be compared with the expected results in Fig. 1. After comparison, it can be concluded that the results are similar.

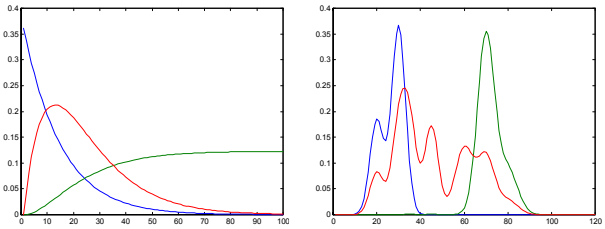

Fig. 5. Concentration profiles and spectral profiles extracted by SIMPLISMA.

7. VARIMAX AND ITTFA

In this section, an ITTFA algorithm in combination with VARIMAX is investigated. The principle on which ITTFA is based is that an initial target is defined and updated until specific criteria are satisfied, Vandeginste *et al*, 1998. The main criteria for success are that appropriate constraints are formulated for updating the targets with realistic initial targets being identified. Targets are adapted by replacing negative values that are produced in the estimated concentration and spectral profiles by zero. Thus for this application, non-negative constraints for the spectra and the concentration profiles are imposed. To select a target, different methods can be used for the initial profiles for each factor including VARIMAX rotation. VARIMAX rotation is based on the principle that the principal components axes can be rotated:

$$\mathbf{F} = \mathbf{V}^T\mathbf{O} \tag{16}$$

where the columns of **V** are the abstract factors of **R** that require to be rotated into real factors.

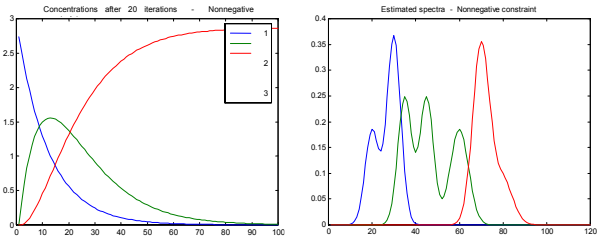

Fig. 6. Final estimates for the concentration and spectral profiles.

The matrix $\mathbf{V}^T$, is rotated by the orthogonal rotation matrix **O** so that the resulting matrix **F** fulfils the criterion that **F** has maximum row simplicity. A measure of simplicity of a vector is the variance of the square of the p elements that are to be maximised. After 20 iterations, the results for the specific reaction can be seen in Fig. 6. These results are compared to the expected results, Fig. 1. From the comparison, it can be concluded that the concentration and spectral profile plots appear to match the expected concentrations

8. INDEPENDENT COMPONENT ANALYSIS

An alternative calibration free resolution method that can be considered is Independent Component Analysis (ICA). ICA can be used to identify the spectral profile of each species in a mixture, i.e. identify the unknown components. ICA is a method designed to offer a solution to the Blind Source Separation problem, i.e. separate the source signals from the observations of their mixtures. ICA can be considered as an extension of PCA in that while PCA identifies principal components that are uncorrelated and that are linear combinations of the observed variables, ICA extracts components (IC's) that are independent and that constitute the observed variables, Hyvarinen *et al*, (2001).

Basically an ICA model is a "statistical latent variable model" in the sense that it describes how the observed data are generated by a process of mixing a number, n, of recorded signals θ. The signals θ are statistically mutually independent by definition and are called independent components (ICs). The basic problem is:

$$\eta_m = a_{m1}\theta_1 + a_{m2}\theta_2 + \ldots + a_{mn}\theta_n, \ \forall \ \ m=1,..,n \qquad (17)$$

where η_m are the observed random variables that are modeled as linear combinations of n random variables θ_m and the a_{ij}, $i, j = 1,\ldots,n$ are real coefficients that are assumed to be unknown. It is also assumed that each mixture η_m and each independent component θ_m are random variables and not time signals or time series. Equation 17 can be rewritten as:

$$\boldsymbol{\eta} = \mathbf{A}\boldsymbol{\theta} \qquad (18)$$

where $\boldsymbol{\eta}$ is a column random vector whose elements are η_m, i.e. if **R** is the data matrix, then n corresponds to each row of **R**, $\boldsymbol{\theta}$ is a column random vector whose elements are θ_m and **A** is a matrix with elements a_{ij}. The statistical estimation problem concentrates on two aspects, under what conditions can the model be estimated and what can be estimated. The answer is that the mixing coefficients a_{ij}, and the ICs, θ_m, must be estimated using the observed variables η_m. For simplicity it is assumed that $\boldsymbol{\eta}$ is a pre-whitened vector, i.e. all its components are uncorrelated and their variances are equal to unity. An alternative way to describe ICA is:

$$\hat{\boldsymbol{\theta}} = \mathbf{M}\boldsymbol{\eta} \qquad (19)$$

where $\hat{\boldsymbol{\theta}}$ is the estimate of $\boldsymbol{\theta}$, η_m is the observed random variable and **M** is a separating matrix which has to be estimated. Matrix **M** can be defined as the weight matrix of a two-layer feed-forward network where $\hat{\boldsymbol{\theta}}$ is the output and $\boldsymbol{\eta}$ is the input. The network is constrained to have statistically independent elements of $\hat{\boldsymbol{\theta}}$, i.e. they have non-Gaussian distributions. Non Gaussianity can be measured by either kurtosis or negentropy.

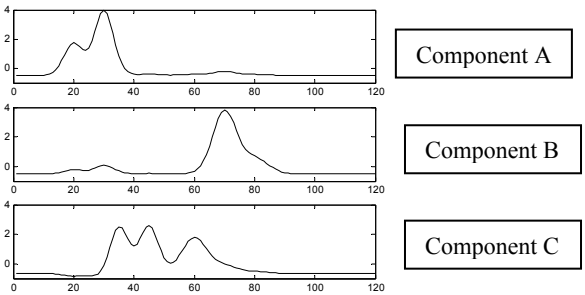

Fig. 7. Estimated spectral profiles using ICA.

The problem of spectral analysis in chemical mixtures represents a very similar problem to that of ICA since it is assumed in spectral analysis that the components of interest are strongly related to the data of the mixture through Beer Lambert's law. Hyvarinen and Oja (1997) have developed an algorithm, FastICA that is used in this paper for the separation of the spectral profiles. Non-gaussianity was a main characteristic of the spectral for this example. The results can be seen in Fig. 8.

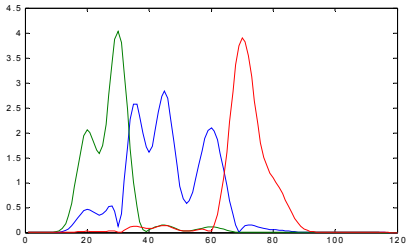

Fig. 8. Results of the application of JADE.

Another ICA algorithm that was also evaluated was the "Joint Approximate Diagonalization of Eigenmatrices" (JADE) (Cardoso, 1999). It is a cumulative-based batch algorithm for source separation. The results can be seen in Fig 8. ICA is

shown to be effective for the analysis of spectral data. The difference in scaling does not affect the qualitative information gained. The main peaks are situated where expected and the components are easily recognisable.

9. JADE AND MCR-ALS

Multivariate Curve Resolution-Alternating Least Squares (MCR-ALS) is a method developed by Tauler (2002). During the procedure, the initial estimates of the concentration profiles or the species spectra are given and then new concentration profiles are calculated by least-squares. In this application, the results from the JADE algorithm were used as an initial estimate of the spectral profiles. The results can be seen in Fig. 9. Compared with Fig. 8, the spectral profiles have clearly improved and the concentration profiles are also reproduced. The constraints of unimodality and non-negativity were imposed. Once the concentration profiles and the pure spectra became stable, the resulting data matrix was resolved.

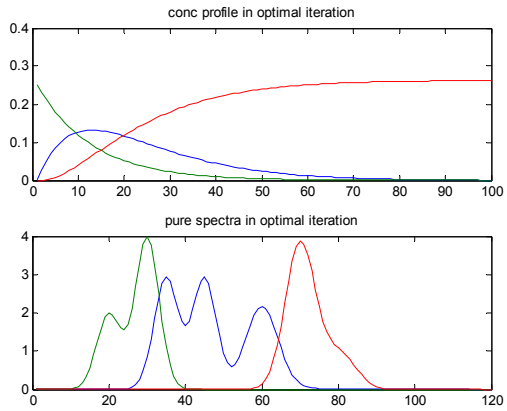

Fig. 9. MCR-ALS with initial estimate by JADE.

10. CONCLUSIONS

A number of calibration-free resolution techniques have been presented. The application of these techniques to an artificially generated spectral data set has demonstrated that they are all effective in terms of its resolution. In addition ICA i.e. both FastICA and JADE can be regarded as another method for the resolution of chemical mixtures. The combination of MCR-ALS and JADE also gave good results. Although the chemical mixture described in this application is simple, ICA has shown that unknown components in a mixture can be identified by the spectra of separated independent components. As an analyst will typically know the range of possible co-existing species in an analytical sample but not the exact number and identities, ICA could prove to be an effective technique. A further advantage of ICA is that it enables the implementation of the resolution of data in limited time. Furthermore ICA could be applied in process monitoring and control and this area is now being considered.

11. ACKNOWLEDGEMENTS

The author would like to acknowledge the EPSRC project KNOWHOW (GR/R/938010) and the EU project BATCHPRO (HPRN-CT-2000-0039) for financial support.

12. REFERENCES

Cardoso, J.F. (1999). High-order contrasts for independent component analysis. *Neural Computation*. **11(1)**, pp. 157-192.

Cuesta Sanchez, F., S.C. Rutan, M.D. Gil Garsia and D.L. Massart (1997). Resolution of multi-component overlapped peaks by the orthogonal projection approach, evolving factor analysis and window factor analysis. *Chemometrics and Intelligent Laboratory Systems*, **36**, pp. 153-164.

Gourvenec, S., D.L. Massart and D.N. Rutledge (2002). Determination of the number of components during mixture analysis using the Durbin-Watson criterion in the orthogonal projection approach and in the SIMLe-to-use interactive self-modeling mixture analysis approach. *Chemometrics and Intelligent Laboratory Systems*, **61**, pp. 51-61.

Hyvarinen, A. and E. Oja (1997). A fast-point algorithm for independent component analysis. *Neural Computation*, **9**, pp. 1483-1492

Hyvarinen, A., J. Karhunen and E. Oja (2001). *Independent component analysis. Adaptive and learning systems for signal processing, communications and contro*l, ed. S. Haykin. John Wiley & Sons.

Keller, H.R. and D.L. Massart (1992). Evolving factor analysis. *Chemometrics and Intelligent Laboratory Systems* **12(3)**, pp. 209-224.

Muller A. and D. Steele (1990). On the extraction of spectra of components from spectra of mixtures. A development in factor theory. *Spectrochimica Acta*. **46(5)** pp. 817-842.

Tauler, R. and D. Barcelo (1993). Multivariate curve resolution applied to liquid chromatography-diode array detection. *Trends in Analytical Chemistry*. **12(8)**, pp. 319-327.

Tauler, R., *MCR-ALS*. 2002, http://www.ub.es/gesq/mcr/theory.htm, http://www.ub.es/gesq/roma/roma.htm

Vandeginste, B.G.M., D.L. Massart, L.M.C. Buydens, S. De Jong, P.J. Lewi and J. Smeyers-Verbeke (1998). *Handbook of Chemometrics and Qualimetrics: Part B*. Elsevier.

STAGE-BASED MULTIVARIATE STATISTICAL ANALYSIS FOR INJECTION MOLDING

Ningyun Lu, Yi Yang, Furong Gao*,

Department of Chemical Engineering
The Hong Kong University of Science & Technology
Clearwater Bay, Kowloon, Hong Kong

Fuli Wang

School of Information Science and Engineering
Northeastern University
Shenyang, Liaoning, P. R. China

Abstract: A multistage based PCA modelling and monitoring approach is demonstrated in this paper to injection molding process, a typical multistage batch process. Analysing the changes of process correlation can lead to effective division of a batch process into several "operation" stages, in good agreement with process knowledge. This shows that multistage based sub-PCA model can be employed not only for effectively process monitoring and fault diagnosis, but also to enhance process understanding.

Keywords: Multivariate statistical analysis, Principal component analysis, Process monitoring, Injection molding, Multi-stage batch process.

1. INTRODUCTION

Batch processes become increasingly preferred choices in chemical industry, to produce higher-value-added products to meet today's rapidly changing market. It is, however, difficult to develop a first-principle or knowledge-based model for process monitoring due to the process high dimensionality, complexity, and batch-to-batch variation, and also due to limited product-to-market time. Multivariate statistical modelling methods, which require only historical process data for analysis and monitoring, and have had many successful applications for continuous processes, are attracting much interest in analysing and monitoring batch processes.

Several statistical modelling methods have been reported recently for batch processes (Wold, et al., 1987; Nomikos and MacGregor, 1994; Dong and McAvoy, 1996; Martin and Morris, 1996; Chen and Liu, 2002), all of which are based on multiway PCA (MPCA), a very popular method for modelling a batch process. These MPCA-based methods, however, are not well-suited for multistage processes because MPCA takes the entire batch data as an object and has difficulty to reveal the changes of process correlation from stage to stage. The on-line application of these MPCA-based methods requires to fill the future unavailable process data in the batch, which can affect the promptness and accuracy of on-line monitoring. Louwerse and Smilde (2000) argued for a strategy to partition reference data into several time periods for improvement of on-line monitoring. But, their method, also based on MPCA, requires also the future measurements unavailable for each remaining time period to be estimated for on-line monitoring. Their method has the same weakness as the MPCA method. Adaptive batch monitoring strategy based on recursive multiblock PCA proposed by Rännar, et al. (1996) can avoid the need of filling the future data. Its computational demand, however, can be overwhelming.

* Corresponding author: E-mail: kefgao@ust.hk; Tel: +852-2358-7139; Fax: +852-2358-0054

Considering that multiplicity of operation stage is an inherent nature of most batch processes, and to alleviate the difficulties of on-line monitoring based on multiway PCA, a stage-based sub-PCA method has been developed by the authors to extend multivariate statistical modelling methods to those multistage batch processes (Lu, et al., 2002). The key to the stage-based sub-PCA monitoring strategy is to divide a batch process into several "operation" stages, according to the changes in process correlation. Within each of these "operation" stages, the process correlation is similar; a representative stage model can be built, using the conventional two-way PCA model. This method allows two-way PCA to be "directly" applied for a batch process.

This paper is to show an industrial application of the proposed stage-based sub-PCA method to a typical multistage batch process, an injection molding process. We will demonstrate that the use of the proposed method can not only improve the ability of process monitoring and fault diagnosis, but also improve the understanding of the process. It is worthwhile to note that the stages defined by the sub-PCA method may be not equal to the real operation stages, as the covariance structure can change during a physical stage. The remainder of the paper is organized as follows: a brief description to the injection molding process is given in Section 2, followed by the introduction of sub-PCA modelling procedures and post data analysis in Section 3. The application of the method for process monitoring and fault diagnosis for injection molding process is described in Section 4. Finally, conclusions are drawn in Section 5.

2. PROCESS DESCRIPTION

Injection molding (Yang and Gao, 1999; Chen, 2002), an important polymer processing technique, transforms polymer materials into various shapes and types of products. Figure 1 shows a simplified diagram of a typical reciprocating-screw injection molding machine with instrumentations.

As a typical multistage process, injection molding operates in stages, among which, injection (or filling), packing-holding, and cooling are the most important phases. During filling, the screw moves forward and pushes melt into the mold cavity. Once the mold is completely filled, the process then switches to the packing-holding stage, during which additional polymer is "packed" at a high pressure to compensate for the material shrinkage associated with the material cooling and solidification. The packing-holding continues until the gate freezes off, which isolates the material in the mold from that in the injection unit. The process enters the cooling stage; the part in the mold continues to solidify until it is rigid enough to be ejected from the mold without damage. Concurrently with the early cooling phase, plastication takes place in the barrel where polymer is melted and conveyed to the front of barrel by screw rotation, preparing for next cycle.

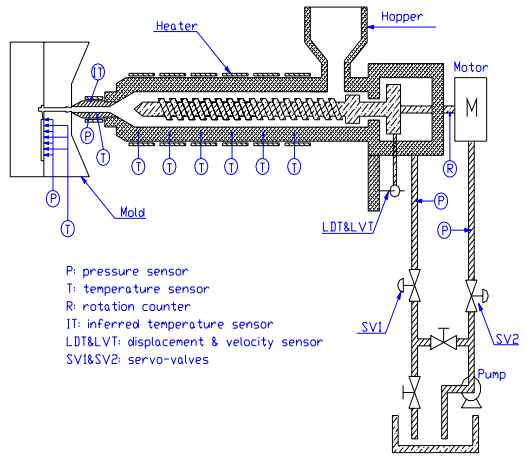

Fig. 1. Simplified illustration of injection molding machine and measuring points

As shown in Figure 1, an injection molding machine like the one in our lab is well instrumented. All key process conditions such as the temperatures, pressures, displacement and velocity can be online measured by their corresponding transducers, providing abundant process information. However, many of these process variables are correlated and time varying. In addition, different stages of operation can lead to different process behaviours, as discussed in detail in the next section. It is an ideal candidate for application of the proposed stage-based multivariate statistical modelling.

For injection molding, high degree of automation is possible. After the process conditions are properly set, the process repeats itself to produce molded part at a high rate. The process is, however, susceptible to the production of off-spec products due to various process malfunctions, drifting of process conditions, changes in materials, and unknown disturbances. Abrupt, gross faults in the key process variables can be easily and reliably detected by the conventional SPC chart. Slow drift or faults involving multiple process variables, however, can be hard to detect. These process faults, even if they are small and not common, can lead to production of large quantity of bad parts, if they are not detected earlier.

The material used in this work is high-density polyethylene (HDPE). The process variables selected for modelling are shown in Table 1. The operating conditions are set as follows: injection velocity is 24mm/sec; mold temperature equals 25ºC; seven-band barrel temperatures are set to be (200, 200, 200, 200, 200, 180, 160, 120) ºC; packing-holding time is

Table 1 Description of the process variables

No.	Variable's description	Unit
1	Nozzle Pressure	Bar
2	Stroke	mm
3	Injection Velocity	mm/sec
4	Injection Pressure	Bar.
5	Plastication Pressure	Bar
6	Injection Cylinder Pressure	Bar
7	Cavity Pressure	Bar
8	Screw Rotation Speed	RPM
9	SV1 opening	%
10	SV2 opening	%
11	Cavity Temperature	ºC
12	Nozzle Temperature	ºC
13	Barrel Temperature 1	ºC
14	Barrel Temperature 2	ºC
15	Barrel Temperature 3	ºC
16	Barrel Temperature 4	ºC

fixed to be 3 seconds with total cycle time around 20 seconds. Totally, 60 normal batch runs are conducted under this operating condition. Another three batch runs are conducted under abnormal conditions for the sub-PCA based process monitoring and diagnosis scheme, as detailed in Section 4.

3. MULTISTAGE SUB-PCA MODELING

3.1. Data pretreatment

Consider a batch process with J process variables measured over sampling points k ($k = 1,2,\cdots,K$); a data matrix of dimensions $J \times K$ is generated from each batch run. A set of I number of normal batch runs hence result in a three-way process data matrix, $X(I \times J \times K)$, which is the most popular data form for batch process.

For the injection molding process as illustrated in this paper, about 1000 measurements for each variable, after removing the meaningless data at the end of each batch run, result in the reference data matrix $X(I \times J \times K)$ of dimension $60 \times 16 \times 1000$. The reference data should be properly scaled before process modelling. Several kinds of scaling methods are argued for the three-way reference data sets by Westerhuis, et al. (2000). For a multistage batch process, different process variables dominate different stages; it is desirable to scale process variables within batch run to retain the inherent weights in different stages. In this work, process variables are normalized by mapping the original measurements into [0,1].

The reference data for batch process is a three-way matrix with three directions standing for batch runs, process variables and sampling points, respectively. To analyse the correlation structure in different batch runs at each sampling time, the reference three-way matrix is unfolded along the time direction, resulting in K number of time-slice matrices, $\tilde{X}^k_{I \times J}$. The conventional two-way PCA method is directly applied to these time-slice matrices to extract the correlation information.

3.2. Multistage sub-PCA modelling

The key to multistage sub-PCA is based on the recognition of the following: (1). a batch process may be divided into several stages, based on its process characteristics; (2). process correlations in two time-slice matrices is similar if the data are sampled within the same stage, despite of the fact that the process may be time varying. The changes of operation stages result in changes of the correlation structures in the time-slice matrix series; also, changes of the correlation may also indicate changes in the process stages.

For each $\tilde{X}^k$, conventional PCA can be applied directly because each batch run can be considered to be independent, and the process variables at time k for each batch run can also be viewed as independent. $\tilde{X}^k$ can then be decomposed by,

$$\tilde{X}^k = \tilde{T}^k (\tilde{P}^k)^T \ (k = 1,2,\cdots,K). \qquad (1)$$

The p-loading matrix, $\tilde{P}^k$, in fact contains the correlation information, which can be used to guide the division of the batch process and to build sub-PCA models. A special designed clustering algorithm is introduced to cluster these K numbers of p-loading matrices, $\tilde{P}^k$ ($k = 1,2,\cdots,K$), into C groups, representing C numbers of "operation" stages for a batch process. Define P_c^* ($c = 1,2,\cdots,C$) as the representative p-loading matrix for the c^{th} stage as,

$$P_c^* = \underset{k}{Min}\left(\left\| \tilde{P}^k - P_c^* \right\|^2 \right) = \frac{1}{n_{stage\_c}} \sum_k \tilde{P}^k \qquad (2)$$

$$(c = 1,2,\cdots,C; k = 1,2,\cdots,n_{stage\_c})$$

where n_{stage_c} stands for the amount of the process data belonging to the stage c.

Similar to that in PCA, P_c^* is divided into two parts, $\bar{P}_c^*$ and $\tilde{P}_c^*$, for principal component subspace and residual space, respectively. In each stage c ($c = 1,2,\cdots,C$), the representative p-loading matrix, P_c^* , is then used to construct a sub-PCA model for stage c as,

$$\begin{aligned} \tilde{T} &= \tilde{X}(\bar{P}_c^*)^T \\ \hat{\tilde{X}} &= \tilde{T}\bar{P}_c^* \\ \tilde{E} &= \tilde{X} - \hat{\tilde{X}} = \tilde{X}(I - \bar{P}_c^*(\bar{P}_c^*)^T). \end{aligned} \qquad (3)$$

The stages may be associated with process time spans if the process is controlled by a time sequence. However, this may lead to occasional mis-grouping of new process data into a wrong stage, due to batch variation. Some characteristic process variables may also be used to better reflect the stage changes, for example, conversion rate for a batch reactor. Alternatively, the control limits at the edges of each stage can be relaxed to reflect the process transient nature from one stage to another.

3.3 Post data analysis

As shown in Figure 2, the p-loading clustering algorithm can divide the process into four main stages and two transient stages according to the change of process correlation. The cooling stage, a long operation stage, actually consists of plastication phase and cooling phase, which can be clearly

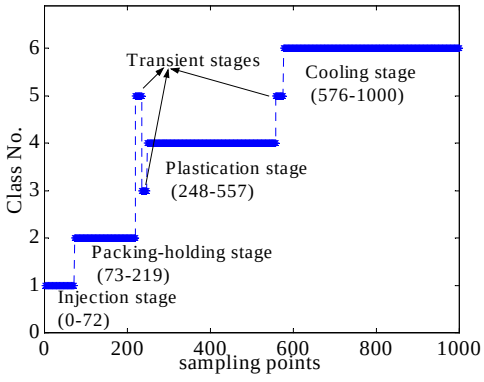

Fig. 2. Stage division of injection molding process by sub-PCA method

Table 2 Sub-PCA models in four operation stages

	Injection stage		Packing stage		Plastication stage		Cooling stage	
	.26	-.11	.36	-.15	.05	-.03	.02	.03
	.20	-.08	.38	-.16	.23	-.12	0	0
	.38	-.17	.01	-.01	.10	-.06	0	0
	.34	-.15	.35	-.15	.06	-.03	.04	.04
	0	0	0	0	.44	-.23	0	0
	.37	-.13	.06	0	0	0	.14	.15
	.02	-.01	.37	-.16	.02	-.01	0	0
*	0	0	0	0	.41	-.22	0	0
	.38	-.18	.27	-.11	.22	-.13	.55	.68
	0	0	0	0	.45	-.25	0	0
	.29	-.14	.34	-.16	.23	-.15	.20	.28
	.30	-.11	.34	-.12	.08	-.02	.10	.09
	.18	.48	.18	.48	.22	.46	.35	-.38
	.20	.49	.19	.50	.22	.47	.38	-.38
	.18	.47	.18	.47	.22	.45	.36	-.33
	.23	.39	.23	.40	.29	.37	.47	-.14
**	90.02		90.51		88.53		84.82	

***** denotes p-loading vectors.

****** denotes the percentage of explained variance by the retained principal components.

divided by sub-PCA method. A few samples in the transient response from packing-holding phase to plastication phase and from plastication phase to cooling phase form two new stages, called transient stage. Four sub-PCA models are then derived for the four main stages. This PCA analysis results in similar stage division to the actual stages used in polymer processing industry, which suggests that the stage division based on the proposed p-loading clustering method can indeed promote the process understanding.

The p-loadings of the stage PCA models are listed in Table 2. The p-loading plots, which are obtained by plotting the second loading vector against the first, indicate the correlation structure of process variables. Variables, located in the same clustering, have high correlation; variables in different clustering have weak relation (Kaspar and Ray, 1992; Yang et al., 2002). As illustrated in Figure 3, process variables (except barrel temperatures) form different clustering in different stage, indicating that these variables have different correlation structures at different stages. The variables located in the circle have small values in the p-loading vectors, indicating that they are

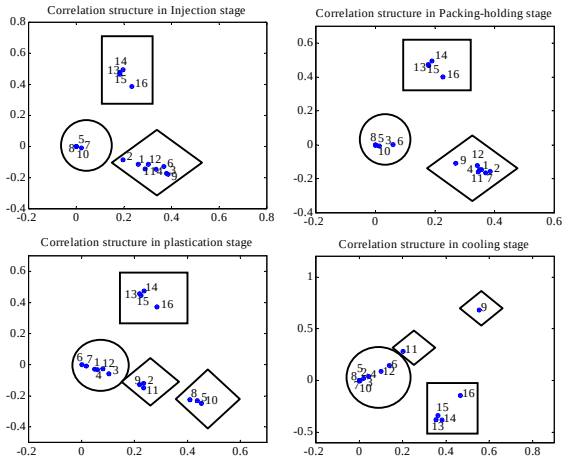

Fig. 3. Correlation structures shown in the p-loading plots. Variables in circle are "unimportant variables"; variables in rectangle are barrel temperatures; variables in diamond are characteristic variables for that stage.

"unimportant" variables for that stage. Variables enclosed by the diamonds and rectangles are dominant variables, have significant contributions to the stage PCA model. All barrel temperatures lie in the rectangle (Variable No. 13, 14, 15 and 16), forming an independent clustering indicating that they have weak relation with other process variables, which will be discussed in detail in Section 4. It is important to point out that variables in the diamonds change from stage to stage, indicating the varying process characteristics and the necessity for a stage based analysis.

4. PROCESS MONITORING AND FAULT DIAGNOSIS BASED ON SUB-PCA MODEL

Statistical process monitoring is conducted based on hypothesis tests on two indices, the *Hotelling-*T^2 and the Q statistics indices (or SPE value), in the principal component subspace and residual subspace, respectively. The confidence region of *Hotelling-*T^2 statistic can be estimated by F -distribution; while Q statistics can be well approximated by a weighted χ^2 distribution (Jackson, 1979, 1991; Westerhuis, et al., 2000). The control limits can be computed following the procedures proposed by Lu et al. (2002). The control limits estimated from I number of normal batch runs describe the normal and systematic variations of the process, provided that the reference process data can cover all normal cases.

On-line process monitoring and fault diagnosis are conducted by judging whether the scores and SPE value of the coming measurements in a running batch are below the control limits. The *Hotelling-* T^2 statistic reveals the abnormality, which can be described by the sub-PCA model; while the Q statistic shows the unexplained information after the process variables being projected onto the principal hyperplane. The process is monitored using the *Hotelling-*T^2 and SPE charts. The batch operation is monitored at every sampling point k with both *Hotelling-* T^2 and SPE monitoring charts. The monitoring procedure first judges which stage the new coming data belongs to, and then call the corresponding sub-PCA model to calculate the values of two indices, *Hotelling-*T^2 and SPE. The values of the two statistics for normal batch runs will be well below the control limits, while abnormal batches may have large values of the *Hotelling-*T^2 and/or SPE statistics. Once an abnormal condition is detected by the monitoring charts, the contribution plot, a commonly-used and effective diagnosis tool, is used to diagnose the fault cause for that stage.

In this work, three typical faults are intentionally introduced. Fault #1 is material disturbance by adding a few grams of polypropylene (PP) into the HDPE. Fault #2 is a barrel temperature sensor failure; while fault #3 is caused by check-ring failure, which is a common problem in injection molding. All faults can change the correlation structure, generating unexplained information by the stage PCA model. They can be promptly detected by the monitoring

charts in the corresponding stage, as illustrated in Figures 4-8.

• *Fault #1*

Material disturbance is the first fault introduced to test the proposed method. A small amount of PP is added to the processing of HDPE. The T^2 and SPE monitoring charts, as shown in Figure 4, indicate that this fault can be identified soon after the starting of filling phase. In terms of the four contribution plots as shown in Figure 5, contamination of a small amount of PP into the HDPE, results in a lower cavity temperature (No. 11) throughout the cycle, as PP cools and solidifies faster than HDPE. At the same time, the viscosity of PP is higher than that of HDPE, which generates larger shear heating for PP, resulting in a higher nozzle melt temperature (No.12). The contribution plot of the packing phase is different from the others. The cavity pressure (No.7) has lower values due to the faster solidification of PP. This characteristic difference among different stages can only be revealed by such a stage-based approach.

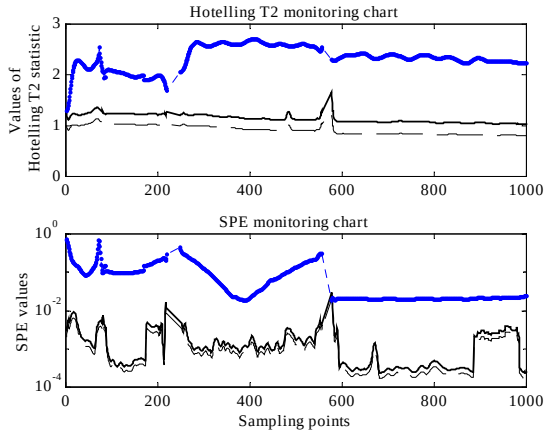

Fig. 4. T^2 and SPE monitoring charts for fault #1.
(Solid line, 99% control limit; dash line, 95% control limit)

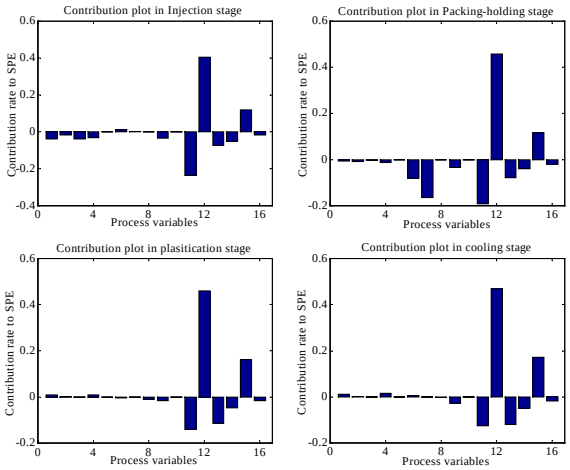

Fig. 5. Contribution plots of the four stages for fault #1

• *Fault #2*

When one thermocouple that measures the barrel temperature fails, the reading of this temperature drops, resulting in full heating of this zone. This creates excessive heats to be conducted to the neighbouring zones, even the heating of those zones are fully shutdown. This change can be quickly picked up by the *Hotelling-*T^2 and SPE monitoring

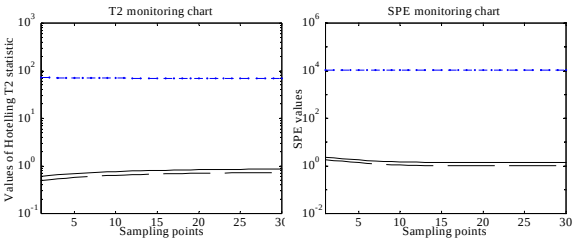

Fig. 6. T^2 and SPE monitoring charts for fault #2.
(Solid line, 99% control limit; dash line, 95% control limit)

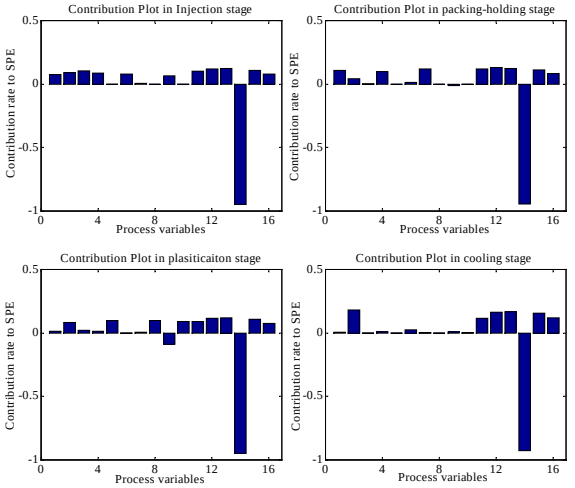

Fig. 7. Contribution plots of the four stages for fault #2

charts as shown in Figure 6. The contribution plots of the four operation stages, shown in Figure 7, clearly indicate the drop of the failed zone temperature (No. 14) and the increased temperatures of the neighbouring zones. The contribution plots in all four stages are similar, because this fault has similar impact on the four stages. As shown in Figure 3, the barrel temperatures (No.13, 14, 15 and 16) form an independent and stable clustering throughout the batch.

• *Fault #3*

The check-ring valve, a device that allows the polymer melt flow from the screw channel to the nozzle during plastication, closes during injection and packing stages to prevent polymer backflow from the nozzle to screw channel. Check-ring failure upsets the process correlations of different stages in different ways. As shown in Figures 8, fault #3 can be readily detected by the SPE monitoring charts. The contribution plots in the first three stages, however, are different, indicating that the fault #3 has different fault characteristics in different stages. The application of stage-based sub-PCA method is advantageous for diagnosing such a fault.

During the filling stage, smaller amount of material will be injected into the cavity, at the same injection velocity, due to the back flow associated with the failure of the checking ring valve. The nozzle pressure (No.1), injection pressure (No.4) and cavity pressure (No.7) are lower, as clearly indicated by the contribution plot of the stage. During the packing-holding phase, more material will have to be packed into the cavity to make up the shortfall in the filling, resulting in a higher stroke (No.2), higher screw speed (No.3), higher pressures (No.4, 5), as expected

from the analysis of the process. This can also be clearly seen in the contribution plot. During plastication, as longer stroke has travelled in filling and packing, a longer plastication stroke (No.2) has to recovered, which is clearly seen in the contribution plot of this stage.

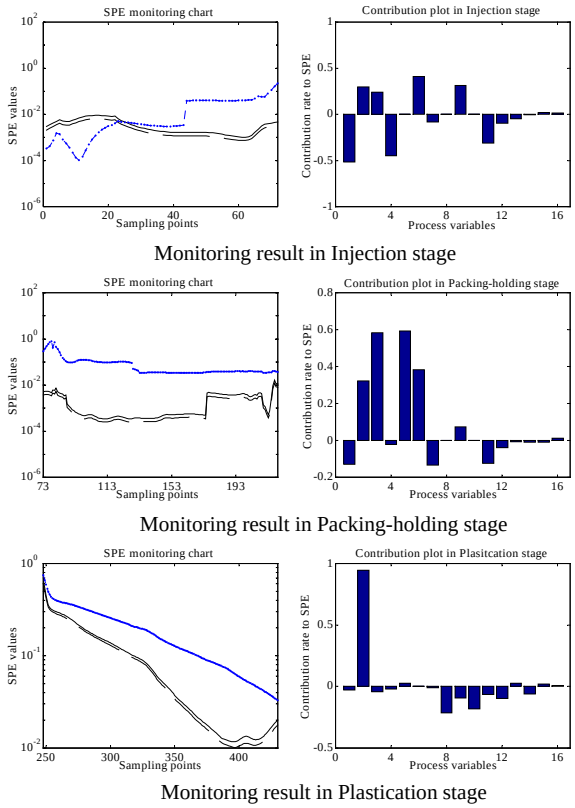

Fig. 8. Monitoring chart and contribution plot for fault #1. (Solid line, 99% control limit; dash line, 95% control limit)

The above analysis is accorded well with the process knowledge of injection molding. For the faults that show different fault characteristics in different stages, it is desirable to analyse the contribution plots of different stages to give a reasonable cause to the fault. This suggests that the application of the sub-PCA modelling method can indeed enhance the process understanding, and improve the ability of fault detection and diagnosis.

5. CONCLUSIONS

A multistage multivariate model has been developed based on the historical data of normal batch runs for injection molding process. This modelling method divides the process into several stages, similar to what is practiced by an injection molding expert. With this multi-stage model structure, the correlation in each operation stage can be analysed in detail to enhance the understanding of the process. The experimental applications indicate that the stage-based sub-PCA modelling is effective for monitoring and detecting process faults. The most possible cause of the abnormality can also be obtained by combining the fault characteristics of different stages. The procedures presented in this paper can provide process operators with a tool for stage-division purely by data analysis. The stage-based monitoring and diagnosis can not only allow on-line monitoring without the need of predicting future data, but also can isolate and identify a fault to a specific stage of the process operation.

REFERENCES

Chen J. and Liu, K. C. (2002). On-line batch process monitoring using dynamic PCA and dynamics PLS models. *Chem. Eng. Sci.*, **57**, 63.

Chen X. (2002). A study on profiling setting of injection molding. *Ph.D. Thesis*, The Hong Kong Univ. of Sci. & Tech., Hong Kong.

Dong D. and McAvoy T. J. (1996). Batch tracking via nonlinear principal component analysis. *J. AIChE*, **42**, 2199.

Jackson J. E. (1991). A User's Guide to Principal Components. Wiley, New York.

Jackson J. E. and G. S. Mudholkar (1979). Control procedures for residuals associated with principal component analysis. *TECHNOMETRICS*, **21**, 341.

Kaspar M. H. and W. H. Ray (1992). Chemometric methods for process monitoring and high-performance controller design, *J. AIChE*, **38**, 1593.

Louwerse D. J. and Smilde A. J. (2000). Multivariate statistical process control of batch processes based on three-way models. *Chem. Eng. Sci*., **55**, 1225.

Lu N., F. Gao and F. Wang (2002) A sub-PCA modeling and on-line monitoring strategy for batch processes. *Submitted to J. AIChE.*

Martin E. B. and A. J. Morris (1996). An overview of multivariate statistical process control in continuous and batch process performance monitoring. *Trans. of Int. Meas. & Cont.*, **18**, 51.

Nomikos P. and MacGregor J. F. (1995). Multivariate SPC charts for monitoring batch process. *TECHNOMETRICS*, **37**, 41.

Nomikos P. and MacGregor J. F. (1994). Monitoring batch processes using multiway principal component analysis. *J. AIChE*, **40**, 1361.

Rännar S., MacGregor, J. F. and Wold, S.(1998). Adaptive batch monitoring using hierarchical PCA. *Chemometrics and Intelligent Laboratory Systems*, **41**, 73.

Westerhuis J. A., Gurden S. P. and Smilde A. K. (2000). Standardized Q-statistic for improved sensitivity in the monitoring of residuals in MSPC. *J. Chemometrics*, **14**, 335.

Wold, S., P. Geladi, K. Esbensen, and J. Ohman. (1987). Multi-way principal components and PLS analysis. *J. Chemometrics*, **1**, 41.

Yang Y. and Gao F. (1999). Cycle-to-cycle and within-cycle adaptive control of nozzle pressures during packing-holding for thermoplastic injection molding. *Poly. Eng. Sci*. **39**, 2042

Yang Y., Lu N., Wang F. and Ma L. (2002). A new fault detection and diagnosis method based on principal component analysis in multivariate continuous processes. *The 4th Proceeding Of the World Congress on Intelligent Control and Automation*, Shanghai, P. R. China, 3153.

NONLINEAR CONTROL OF A BATCH REACTOR IN THE PRESENCE OF UNCERTAINTIES

H. Sibarani * **Y. Samyudia** *,[1] **P. L. Lee** **

* *Department of Chemical Engineering, McMaster University, Hamilton, ON, Canada.*
** *Division of Engineering, Science and Computing, Curtin University of Technology, Perth, Australia.*

Abstract: In this paper, we propose new control design strategies within the Generic Model Control (GMC) framework for tracking the pre-determined temperature profiles of a batch reactor. It is shown by simulation studies that the designed robust GMC controller is able to track the temperature reactor profile reasonably well, and its optimal performance is maintained in spite of large uncertainties.

Keywords: batch reactor, nonlinear control, uncertainties

1. PROBLEM FORMULATION

In recent years, the optimization, monitoring and control of batch processes have been an active research area as the emergence of generic drugs from the pharmaceutical industries are now pushed to be the first on the market (Bonvin, 1997; Y. Yabuki and MacGregor, 2002). A batch reactor is a typical process that exhibits challenging operational problems because of its highly nonlinear dynamics and its complex reaction kinetics and stoichiometry. As a result, the use of model-based technology to optimally operate the batch reactor should address simultaneously the nonlinear dynamics and the modelling errors due to the inability to model such complex reactions.

The operation of a batch reactor typically employs a process optimization and feedback control arrangement (Jutan and Uppal, 1984; M.V. Le Lann, 1999). Models are used in both optimization and control. Different approaches have been pursued to obtain a reliable kinetic and stoichiometric model. A *tendency modelling* has been the popular approach to capture the kinetics and stoichiometric of the reaction (C. Filippi and Georgakis, 1986). The minimum necessary and essential data for the reaction model development are: the total batch data, the reactor temperature, the initial compositions and the final concentration of different components. The model is used for the optimization of the batch operation to maximize either yields or some economic factors subject to some process constraints (e.g. rate of change in temperature, heat generated, etc.). The batch optimization is aimed at determining the temperature or additional reactant rate profiles. The profiles should be tracked optimally by the feedback control implemented for each batch cycle. Due essentially to the lack of on-line concentration measurements, in practice the problem of batch reactor control remains a problem of temperature control. Thus, the control performance is mainly dependent on the heating-cooling systems associated with the reactor.

We consider a batch reactor studied in (C.Kravaris and Chung, 1987). In the batch reactor, the following consecutive reaction is taking place:

[1] Corresponding author: samyudi@mcmaster.ca. This work was supported by NSERC grant no. 249513-02 and McMaster Steel Research Center.

$$A \xrightarrow{k_1} B \xrightarrow{k_2} C \tag{1}$$

and the reaction model is given as:

$$\begin{aligned} \frac{dC_A}{dt} &= -k_1(T)C_A^2, \\ \frac{dC_B}{dt} &= k_1(T)C_A^2 - k_2(T)C_B, \end{aligned} \tag{2}$$

with the initial concentrations of A and B are $C_A(0) = 1$ and $C_B(0) = 0$, and some parameters are defined as:

$$\begin{aligned} k_1(T) = A_{10}e^{(-E_1/RT)}; k_2(T) = A_{20}e^{(-E_2/RT)}; \\ A_{10} = 1.1;\ E_1 = 2.09 \times 10^4; \\ A_{20} = 172.2;\ E_2 = 4.18 \times 10^4; \\ R = 8.31 \times 10^{-3};\ T_{min} = 25^oC;\ T_{max} = 125^oC \end{aligned}$$

Batch cycle time is 1 hr. Within this cycle time, the feedback controller should be able to track the following reactor temperature profile $T_d(t)$, which is produced by the batch optimizer:

$$T_d(t) = 54 + 71e^{-2.5\times10^{-3}t}\ ^oC \tag{3}$$

subject to some operational constraints and uncertainties.

The critical step in designing the batch temperature control system is the choice of manipulated variable. The reactor temperature T can be controlled by regulating the steam temperature supplied into the heating jacket T_s and the flow rate of the coolant in the cooling coil F_c. The heat balance equation is:

$$\begin{aligned} \rho C_p V\frac{dT}{dt} &= k_1(T)C_A^2(-\Delta H_1)V + k_2(T)C_B(-\Delta H_2)V \\ &\quad + U_jA_j(T_s - T) - U_cA_c(T - T_c) \\ \frac{1}{U_c} &= \frac{1}{4550F_c^{0.8}} + \frac{1}{10.8} \end{aligned} \tag{4}$$

There are two manipulated variables, T_s and F_c available for controlling the reactor temperature T. We will use a single parametric variable u as a combined manipulated variable for the temperature control, where u is defined as (Jutan and Uppal, 1984):

$$\begin{aligned} T_s &= (T_{s,max} - T_{s,min})u + T_{s,min} \\ U_c &= (U_{c,min} - U_{c,max})u + U_{c,max} \end{aligned} \tag{5}$$

where the maximum and the minimum value of T_s and U_c are selected from the safety limits. Obviously, $u = 0$ denotes maximum cooling of the system while $u = 1$ represents the maximum heating. By substituting (5) into (4) and after some arrangement, we obtain:

$$\begin{aligned} \frac{dT}{dt} &= \gamma_1 k_1(T)C_A^2 + \gamma_2 k_2(T)C_B \\ &\quad + (a_1 + a_2T) + (b_1 + b_2T)u \end{aligned} \tag{6}$$

where the parameters are defined as:

$$\begin{aligned} &\gamma_1 = (-\Delta H_1)/\rho C_p,\ \gamma_2 = (-\Delta H_2)/\rho C_p \\ &a_1 = (U_jA_jT_{s,min} + U_{c,max}A_cT_c)/\rho C_pV \\ &a_2 = -(U_jA_j + U_{c,max}A_c)/\rho C_pV \\ &b_1 = [U_jA_j(T_{s,max} - T_{s,min}) - (U_{c,max} - U_{c,min})A_cT_c]/\rho C_pV \\ &b_2 = (U_{c,max} - U_{c,min})/\rho C_pV \end{aligned}$$

and the constants are chosen as:

$$\begin{aligned} &\rho C_p = 1000,\ \Delta H_1 = -4.18 \times 10^4;\ \Delta H_2 = -8.36 \times 10^4; \\ &A_j/V = 30,\ A_c/V = 17,\ U_j = 1.16 \end{aligned}$$

The operational constraints are given by

$$\begin{aligned} &T_{s,max} = 150,\ T_{s,min} = 70,\ T_c = 25 \\ &F_{c,max} = 33.1 \times 10^5,\ F_{c,min} = 4.8 \times 10^5 \end{aligned} \tag{7}$$

Uncertainties in the batch reactor could be in terms of uncertain initial concentration of $A, C_A(0)$, reaction constants A_{10} and A_{20}, and the activation energies E_1 and E_2. Hence, the batch temperature control problem is formulated as follows: *Design a nonlinear controller that is able to track the temperature profile given in (3) subject to process constraints in (7) and large uncertainties in the initial concentration of A, reaction constants and the activation energies.*

In this work, we present a new robust Generic Model Control (GMC) design framework to optimally track the pre-determined temperature profile in the presence of uncertainties. The method is developed by optimizing the GMC parameters (τ and ξ) for the desired robust stability and performance levels.

2. STANDARD AND ROBUST GMC DESIGN

2.1 Standard GMC Design

GMC is a class of nonlinear control design that makes use of: a dynamic (nonlinear) model of a process, a reference system in terms of a desirable rate of change of the output variables, and a generation of an optimal control law to ensure closed-loop performance. A dynamic (nonlinear) model of the process is described as a set of differential equations:

$$\frac{dy}{dt} = f(y, u, d, \theta) \tag{8}$$

where y, u and d are the vectors of model outputs, inputs and measured disturbance variables, and θ is a vector of known process parameters. In general, f is a vector of known (or approximation of) nonlinear functional relationships of those variables. We never obtain an exact representation of the plant using (8). In other words, *process/model mismatch* inherently occurs when

applying the GMC design, like other model-based design methods. The mismatch could be in the forms of structural mismatch (i.e. $f(.)$ is the result of model simplification) and/or parametric mismatch (i.e. θ represent partially known process parameters).

The basic idea of GMC design is to apply a reference system as a desirable rate of change of the controlled variables, $(\frac{dy}{dt})^*$. One reasonable choice of the reference system is:

$$(\frac{dy}{dt})^* = K_1(y^{sp} - y_o) + K_2 \int_0^\tau (y^{sp} - y_o)dt \quad (9)$$

Lee (Lee and Sullivan, 1988) discussed how the parameters K_1 and K_2 were chosen using simple techniques to accommodate the desired closed-loop performance. For example, to determine the i^{th} element of the diagonal matrices K_1 and K_2, the following simple rules can be applied:

$$k_{1i} = \frac{2\xi_i}{\tau_i}; \quad k_{2i} = \frac{1}{\tau_i^2} \quad (10)$$

The parameters ξ_i and τ_i specify the shape and speed of the desired closed-loop trajectory of the i^{th} controlled variable. It is obvious that the parameters of τ and ξ captures the desired closed-loop performance of GMC. No robustness objective is explicitly considered during the choice of K_1 and K_2. In the standard GMC design procedure, the robustness objective has been considered indirectly, and often in ad-hoc manner. No systematic procedure is available to explicitly address the robustness objective.

By combining (9) and (8), the optimal GMC inputs, u^{opt} are generated by solving a minimization problem formulated as:

$$u^{opt} = arg\min_u \; J_{GMC} = \int_0^\tau \epsilon^T(t)\epsilon(t)\; dt \quad (11)$$

subject to: $u \in \mathcal{U}$. The objective function is defined as:

$$\epsilon(t) = [f(y_o, u, d, \theta) - (\frac{dy}{dt})^*] \quad (12)$$

The GMC control law is hence implemented as solving the optimization problem numerically at every sampling time by employing the model (8). Alternatively, an explicit solution of (11) is also possible only if the model (8) satisfies the nonlinear invertibility conditions.

2.2 Robust GMC Design

Consider the situation where there is no process/model mismatch and the nonlinear model (8) is completely invertible. This situation is referred to as the *ideal* case. In this ideal case, the dynamics from the reference rate of the process output change $\left(\frac{dy}{dt}\right)^*$ to the process output y_o (or *internal dynamics*) follows a pure integrator system $G = \frac{I}{s}$. The ideal closed-loop system is given by:

$$y_o = (sI - K)^{-1}K\; y^{sp} \quad (13)$$

where K is the diagonal transfer function matrix. This result shows a perfect disturbance rejection and decoupling of the outputs. Also, the stability and performance of the closed-loop system is dependent on $(sI - K)^{-1}K$. For the standard GMC design, the ideal closed-loop system (13) corresponds to a linear system $G = \frac{I}{s}$ under K, which corresponds to a PI controller (9).

The closed-loop analysis of the ideal case leads to the choice of a nominal model for designing an *optimally robust* GMC reference trajectory, K_{opt}. Samyudia and Lee (Samyudia and Lee, 2002) have used the integrator system $G = \frac{I}{s}$ as a nominal model, and then applied the H_∞ loop shaping design of McFarlane and Glover (McFarlane and Glover, 1992) for deriving K_{opt}, which is formulated as:

$$\left(\frac{dy}{dt}\right)^* = WK_\infty(y^{sp} - y_o) = K_{opt}(y^{sp} - y_o) \quad (14)$$

The stable transfer function matrix K_∞ is derived by minimizing the H_∞ norm of the following closed-loop transfer matrix:

$$H(G_s, K_\infty) = \begin{bmatrix} -SG_s & S \\ -K_\infty SG_s & K_\infty S \end{bmatrix} \quad (15)$$

where $S = (I - G_sK_\infty)^{-1}$ and $G_s = GW$. The elements of diagonal weighting function W follows a PI structure as:

$$w_i = \frac{k_i(s + z_i)}{s} \quad for\; i = 1, \cdots, n_y \quad (16)$$

where n_y is the number of outputs. Note that the choice of k_i and z_i can follow the simple rules of (10).

The GMC controller with the robust reference trajectory K_{opt} achieves an optimal robust stability margin $b_{[G,K_{opt}]} \leq \| H(G_s, K_\infty) \|_\infty^{-1}$.

In the presence of process/model mismatch, the internal dynamics can be different from $G = \frac{I}{s}$, say G_p. The robust closed-loop stability is determined using the following proposition:

Proposition 1. (Samyudia and Lee, 2002) Let $G = \frac{I}{s}$ be a nominal model for designing a robust GMC reference trajectory with a robust stability margin $b_{[G,K_{opt}]}$. The closed-loop system of GMC in the presence of process/model mismatch is guaranteed to be stable if and only if $b_{[G,K_{opt}]} > \delta_\nu(G, G_p)$, where G_p is the actual internal dynamics.

Proposition 1 was derived as a direct application of the robust stability conditions in terms of ν-gap metric (Vinnicombe, 1993). There are two

interesting points to make concerning Proposition 1. Firstly, the smaller $\delta_\nu(G, G_p)$, the closer the achieved performance of the GMC controller would be to the ideal closed-loop performance as in (13). Secondly, for a specified performance objective as represented by the weighting function W, the robust reference trajectory of the GMC controller, K_{opt} can be designed for the maximum robustness level, $b_{opt} = \| H(G_s, K_\infty) \|_\infty^{-1}$.

Given the features of the robust GMC reference trajectory, K_{opt}, our new design methods are developed for the standard GMC controller, where the parameters τ and ξ are optimally adjusted such that (9) approximates K_{opt}. This attempt is motivated by the current practice that the GMC parameters τ and ξ are often adjusted in an ad-hoc manner to maintain the GMC performance in the presence of process/model mismatch. Our contribution of this work is therefore to establish a systematic procedure to optimally tune the GMC parameters τ and ξ such that the standard GMC controller satisfies the robustness objective.

2.3 Standard GMC Design for Optimal Robustness

As presented in Section 2.2, the robust GMC reference trajectory K_{opt} is different from the standard GMC reference trajectory because of the additional term K_∞. Since (9) and (14) are linear systems, we can measure their distance using the ν-gap metric as: $\delta_\nu(K_{opt}, K)$, where the ν-gap metric is a normalized measure that spans between zero and one. The smaller the distance, the closer the robustness of the standard GMC controller would be to the robust GMC controller with K_{opt}. This result leads to a systematic tuning of the standard GMC parameters τ and ξ for achieving an optimal robustness. The optimal GMC tuning is formulated as follows:

Procedure 1. Find the GMC parameters τ and ξ that minimize $\delta_\nu(K_{opt}, K)$, or mathematically:

$$\min_{0<\tau<\tau_H, 0<\xi<\xi_H} J_{RS} = \delta_\nu(K_{opt}, K(\tau, \xi)) \quad (17)$$

subject to: $J_{RS} < b_{opt}$.

This procedure can be applied for a given K_{opt}. The upper bounds, τ_H and ξ_H, are set by considering the closed-loop performance limits (e.g. speed and shape of responses). A reasonable set on the upper bounds τ_H and ξ_H makes the optimization problem convex. For the optimal values of τ^* and ξ^*, the achieved robustness of the standard GMC controller, b_{GMC} is guaranteed by:

$$\delta_\nu(G, G_p) < [b_{opt} - \delta_v(K_{opt}, K(\tau^*, \xi^*))] \approx b_{GMC} \quad (18)$$

where the ν-gap metric between the nominal model G and the actual internal dynamics G_p measures the process/model mismatch. Hence, by applying the new design procedure of (17), we are able to accommodate the robustness objective within the standard GMC design procedure by optimally tuning the parameters τ and ξ to satisfy the robust stability objective.

Note that translating $\delta_\nu(G, G_p)$, for example, to the range of parameter mismatch, however, would be difficult and be case-dependent. Our effort to estimate the actual process/model mismatch is to employ a closed-loop metric, which is calculated from a set of closed-loop data in response to a bounded power disturbance. For the worse-case disturbances, this metric is equivalent to $\delta_\nu(G, G_p)$.

2.4 Standard GMC Design for Robust Performance

The most important objective of any controller design is to maintain its ideal performance in spite of the presence of process/model mismatch. This is known as a *robust performance* objective. When designing the GMC controller for robust performance, the achieved closed-loop performance should be quantified and compared with the ideal performance. Hence, to achieve the robust performance property, we require a set of actual closed-loop data from which we compute a closed-loop metric as a measure of robust performance. So, the closed-loop metric is defined as:

$$\delta_\nu(\tau, \xi) := \frac{\| z(\tau, \xi) - z^* \|_S}{\| r \|_S} \quad (19)$$

where $z = \begin{bmatrix} y & \frac{dy}{dt} \end{bmatrix}^T$ is the measured data from the achieved closed-loop system where the plant is running under the standard GMC controller, $z^* = \begin{bmatrix} y^* & \frac{dy^*}{dt} \end{bmatrix}^T$ is the simulated data generated from the ideal closed-loop system where the robust GMC with K_{opt} is running for the nominal model G, r represents a typical disturbance, and $\| \cdot \|_S$ denotes a bounded power (semi-norm) of a signal.

Since the closed-loop metric is evaluated for a particular disturbance r, this metric is not equivalent to $\delta_\nu(G, G_p)$. Recently, Date (Date, 2000) has shown that $\delta_\nu(G, G_p) := \sup_{r \in S_r} \delta_\nu(\tau, \xi)$, where S_r is a set of ℓ_∞^1 bounded signals. The ν-gap metric is therefore equivalent to the closed-loop metric evaluated for the worst-case disturbances. If we could identify what the worst case disturbances would be, and apply them to both achieved and ideal closed-loop loop systems, then the closed-loop metric in (19) would approach $\delta_\nu(G, G_p)$. This implies that we should have $\delta_\nu(\tau, \xi) \leq \delta_\nu(G, G_p)$.

This result has an interesting implication to our GMC design. The GMC parameters τ and ξ

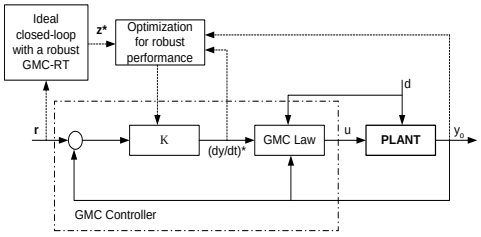

Fig. 1. GMC control design for robust performance

can now be obtained for a robust performance objective in response to the disturbance r.

Procedure 2. An optimal design of the standard GMC controller for robust performance with respect to a disturbance r follows a two step procedure as:

(1) Design a stabilizing GMC controller using either (17) or Lee and Sullivan's method.
(2) Re-tune the GMC parameters τ and ξ by solving the following optimization:

$$\min_{\tau>0,\xi>0} \; J_{RP} = [\delta_\nu(\tau,\xi) + \delta_\nu(K_{opt}, K(\tau,\xi))] \tag{20}$$

subject to: $J_{RP} < b_{opt}$.

The constraint represents the robust stability condition, which means that the robust performance objective is achieved only if the robust stability condition is satisfied. Also, the constraint is to guarantee that we have a stabilizing controller at each iteration when solving the optimization (20).

By following the above two step procedure, the achieved robust performance level is indicated by $J_{RP}(\tau^*, \xi^*)$, where τ^* and ξ^* are the optimal solutions to the optimization problem of (20). The smaller $J_{RP}(\tau^*, \xi^*)$ as compared to b_{opt}, the closer the achieved closed-loop performance would be to the ideal closed-loop performance. This means that the controller can effectively handle the process/model mismatch. Fig. 1 illustrates a schematic diagram of the robust GMC controller. The outer loop is a data-driven optimizer to optimally tune the GMC parameters τ and ξ by solving the optimization problem (20). The inner loop is the closed-loop system where a (*to be updated*) GMC controller is implemented in the actual plant. Both loops are running at different sampling rates, where the inner loop is running faster than the outer loop.

The process noise or unmeasured disturbance are assumed to be uncorrelated with the excitation signal r. Also, the power of the excitation signal is large enough to ensure a high signal to noise ratio.

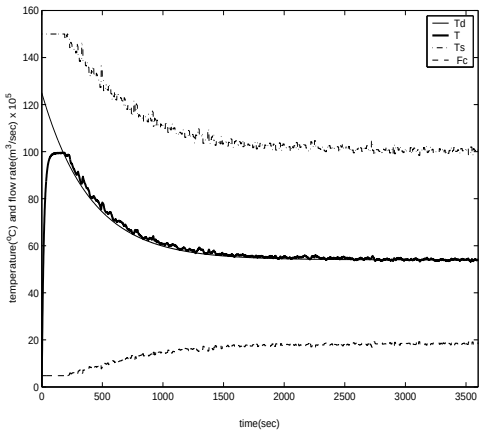

Fig. 2. Robust GMC controller with K_{opt}.

3. APPLICATION TO THE BATCH REACTOR

The new GMC design procedures were applied to the batch temperature control problem. In the simulation, we applied a $\pm 100\%$ uncertainty in the initial concentration of A, $C_A(0)$ and the reaction constants, A_{10} and A_{20}, and a $\pm 50\%$ uncertainty in the activation energies E_1 and E_2. In the GMC nonlinear model, the concentration dynamics were not considered. Further, measurement noise was introduced as a zero-mean random numbers with variance 25, and a zero-mean random numbers with variance 0.056 was added to the heat balance equation.

Fig. 2 shows the ideal responses of the robust GMC controller with K_{opt}, which was designed for an optimal robustness b_{opt}=0.705. The responses are reasonably good in tracking the temperature profile while satisfying the operational constraints.

The responses of the standard GMC controller with the parameters $\tau = 141.4$ and $\xi = 1.07$, are presented in Fig. 3. The responses are stable, but worse and more sensitive to noise as compared to the responses of the robust GMC (or RGMC). To improve the performance of the standard GMC controller, we applied Procedure 1. The optimization process is shown in Fig. 4. The optimal GMC parameters were obtained as $\tau^* = 140$ and $\xi^* = 7.00$. The responses of the optimal robustly tuned GMC controller are presented in Fig. 5. The responses are improved significantly and achieve almost the same responses as the RGMC controller.

The effect of different initial GMC parameters when solving the optimization of Procedure (2) was also investigated. For example, another set of initial GMC parameters was chosen as $\tau = 100$ and $\xi = 7.07$. Then, the same optimal GMC parameters $\tau^* = 140$ and $\xi^* = 7.00$ were obtained. This indicates the convexity of the optimization

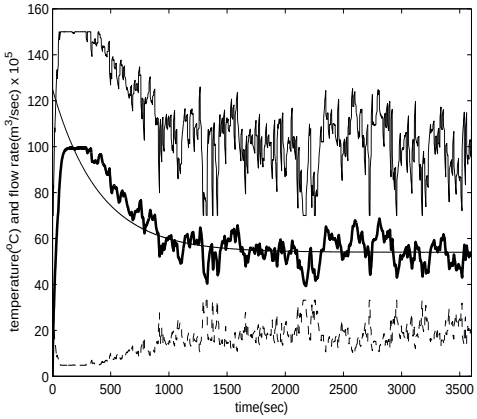

Fig. 3. Standard GMC controller.

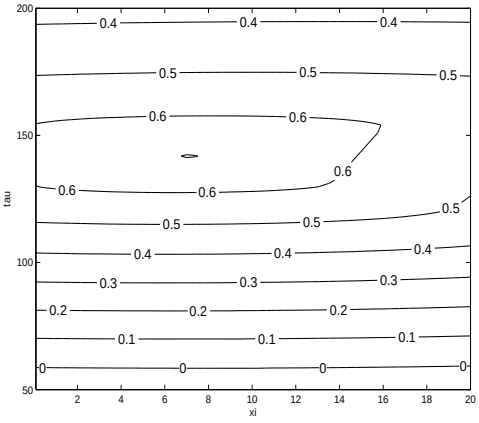

Fig. 4. Contour $b_{GMC(\tau,\xi)}$.

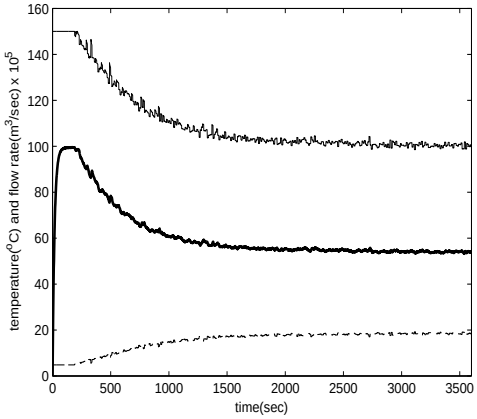

Fig. 5. Optimally tuned GMC controller

problem in (14). This is partially because of the reasonable choice of τ_H and ξ_H.

The GMC design procedure for robust performance was then followed for the batch temperature control problem. The optimization process is depicted in Fig. 6. The optimal parameters were obtained as $\tau^* = 140$ and $\xi^* = 7.00$, which are the same as obtained for robust stability. This result shows that for the batch reactor control problem, the optimal GMC parameters for robust stability achieve a robust performance property. As indicated by a faster change of the optimization

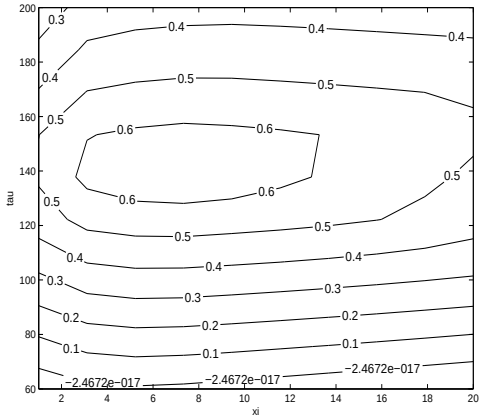

Fig. 6. Contour $(b_{opt} - J_{RP})$

contour in Fig. 6 than in Fig. 4, the feasible range of the GMC parameters for robust performance is smaller than that for robust stability.

4. CONCLUSIONS

With the application to a batch reactor control problem, new procedures to the robust nonlinear GMC control design have been presented in this paper. The new design procedures have been used to robust optimally tune the standard GMC parameters. As shown by simulation studies, the performance of robust nonlinear GMC controllers was reasonably well in tracking the batch reactor's temperature trajectory in spite of the presence of large uncertainties in the initial conditions and process parameters.

REFERENCES

Bonvin, D. (1997). *IFAC ADCHEM* pp. 459–493.

C. Filippi, J.L. Graffe, J. Bordet J. Villermaux J.L. Barney P. Bonte and C. Georgakis (1986). *Chem. Eng. Sci.* **41**, 913–920.

C.Kravaris and C.B. Chung (1987). *AIChE Journal* **33 (4)**, 592–603.

Date, P. (2000). *PhD Thesis*. Univ. of Cambridge, UK.

Jutan, A. and A. Uppal (1984). *Ind. Eng. Chem. Process Des. Dev.* **23**, 597.

Lee, P.L. and G. Sullivan (1988). *Computers & Chem. Engineering* **12**, 573–580.

McFarlane, D.C. and K. Glover (1992). *IEEE Trans. Auto. Control* **37 (6)**, 759–769.

M.V. Le Lann, M. Cabassud, G. Casamatta (1999). *Annual Reviews in Control* **23**, 25–34.

Samyudia, Y. and P. L. Lee (2002). A practical approach to robust nonlinear control design. *Int'l J. of Robust and Nonlinear Control*.

Vinnicombe, G. (1993). *IEEE Trans. Auto. Control* **38**, 1371–1383.

Y. Yabuki, T. Nagasawa and J.F. MacGregor (2002). *Comp. & Chem. Eng.* **26**, 205–212.

Modeling and Model Based Feeding Control for *Pichia pastoris* fed-batch cultivation

Ren H. T.[1], Deng J. H.[2], He B.K.[2], Ren L.M. [2], Yuan J.Q.[1,3,*]

1 Department of Automation, Shanghai Jiao Tong University, 200030 Shanghai, PR China
2 New Drug Research and Development Center, North China Pharmaceutical Company, 050015 Shijiazhuang, PR China
3 State Key Laboratory of Bioreactor Engineering/ECUST, 200237 Shanghai, PR China

Abstract: A structured kinetic model, which takes account of major metabolic pathways of glycerol and methanol in *Pichia pastoris*, is presented. Based on the combined kinetic and bioreactor model, feeding profiles of methanol are determined with the aim of maintaining constant specific growth rate during production stage. Compared with the decreasing type of specific growth rate resulted from constant feeding profile in the standard protocol, the constant specific growth rate is believed to be advantageous for improving the productivity. Experimental results indicate that simulations of biomass and protein concentration agree well with the measured data, and the specific growth rates were successfully controlled at various set points.

Keywords: *Pichia pastoris*, Fed-batch cultivation, Modeling, Feeding profile, Model based control

1. Introduction

The specific growth rate of microorganisms has been found to have prominent influence on the productivity in bioprocesses (Jimenez, *et al*., 1997; Chung, 1999). d'Anjou, *et al*. (1997) developed a mass balance and Monod type kinetic model for *P. pastoris* expressing sea raven anti-freeze protein (SR-AFP). Although the measurements agreed with model simulations only qualitatively, the growth associated product formation was revealed. Based on a mass balance model, Kobayashi, *et al*. (2000) obtained the optimal specific growth rate for *P. pastoris* expressing recombinant human serum albumin (rHSA) by dynamic programming method. In the work of Jahic, *et al*. (2002), a kinetic model for *P. pastoris* expressing a fusion protein was proposed to describe cell growth and oxygen consumption. They found that the productivity could be increased by increasing the specific growth rate. In this paper, a structured model for *Pichia pastoris* expressing rHSA is constructed based on the analysis of metabolic pathways of glycerol and methanol. With this model, methanol feeding strategy during production stage is investigated. The aim is to control the specific growth rate at desired set points.

2. Process Description

Recombinant human serum albumin is expressed by *P. pastoris* GS115. The inoculum was grown for 12 to 24 hours until OD_{600} reached 2 to 6. 5-10% inoculum was used for inoculation. Cultivations were carried out in a 30L bioreactor (B.Braun, Germany) with a working volume of 20L at 30℃. pH was maintained at 6.5 by adding 25% ammonia solution, and DO at 30% by adjusting agitation. The solutions of glycerol and methanol were fed with calibrated peristaltic pumps (Watson 101, England). The medium composition was the same as Boze, *et al*. (2001) used.

* Corresponding author
Tel.: +86-21-62932031.E-mail: jqyuan@sjtu.edu.cn

The cultivation included a glycerol phase and a methanol phase. The glycerol phase was divided into a batch stage and a fed-batch stage. Cultivation began with the batch stage. Upon the depletion of the glycerol in the batch medium, fed-batch stage commenced by adding glycerol solution at predetermined feeding rates. The glycerol fed-batch culture lasted 16-20 h in order for obtaining high cell density. The methanol phase was subdivided into a 10 h induction stage and a production stage. In the induction stage, methanol was fed with a low initial value in order for the cells to adapt the shifting of carbon source. The majority of rHSA was yielded in the production stage. To determine biomass and protein concentration, samples were collected at intervals of 2 h in the glycerol phase and 4 h in the methanol phase, respectively. Biomass concentration in wet weight was routinely measured. Methanol concentration was measured by HPLC, and the concentration of rHSA was measured with 2D-electrophoresis.

3. Modeling and Validation

3.1 Metabolic flux in the glycerol phase

In the glycerol phase, the main metabolic pathways include phosphorylation, glycolysis, TCA cycle and respiratory chain. The balance equations describing fluxes of metabolites, ATP and NADH in these pathways are presented in Eqs. (1); (2); (4) and (5); (7), respectively (Gancedo, *et al*, 1968; Nevoigt and Stahl, 1997). The formation of the byproduct ethanol (Sonnleitner and Kaeppeli, 1986; Ratledge and Kristiansen, 1987) was neglected in this model for simplification. Eqs. (3) and (6) present the main flux of biomass formation. The assumption was made that ATP was consumed mostly for cell growth and maintenance, as described in Eq. (8). The meaning of the symbols appearing in these equations is explained in the nomenclature.

$$S_{Gly} \xrightarrow{q_{Gly}} S_{GP} \tag{1}$$

$$S_{GP} \xrightarrow{r_S} Pyruvate + ATP + 2NADH \tag{2}$$

$$S_{GP} \xrightarrow{\mu K_{B1}} Cell\ material \tag{3}$$

$$Pyruvate \xrightarrow{r_{Ac}} Acetyl\text{-}CoA + NADH + CO_2 \tag{4}$$

$$Acetyl\text{-}CoA \xrightarrow{r_{TCA}} 2CO_2 + ATP + 4NADH \tag{5}$$

$$Acetyl\text{-}CoA \xrightarrow{\mu K_{B2}} Cell\ material \tag{6}$$

$$1/2O_2 + NADH + P/O\,ADP \xrightarrow{r_{NAD}} P/O\,ATP \tag{7}$$

$$r_{ATP} = \frac{\mu}{Y_{ATP}} + m_{ATP} \tag{8}$$

3.2 Metabolic flux in the methanol phase

In the methanol phase, methanol is first oxidized to formaldehyde (Gellissen, 2000), as described in Eq. (9). The assumption was made that the majority of formaldehyde was condensed with xylulose 5-monophosphate to form glyceraldehydes 3-phosphate (GAP) in an assimilatory pathway, as presented in Eq. (10), where three molecules of formaldehyde are consumed to produce one net molecule of GAP (Gellissen, 2000; Lueers, *et al*., 1998; Cereghino and Cregg, 2000). The rest part is oxidized to formate, and further dissimilated to CO_2 with the generation of reducing power NADH. This is described with Eq. (11). The ratio of formaldehyde catalyzed between dissimilation and assimilation, denoted by φ, is being under investigation. Here, φ was set to 0.25. For simplification, biomass formation was mathematically assumed to be resulted from formaldehyde, see Eq. (12), although it is from GAP metabolically (Gellissen, 2000; Lueers, *et al*., 1998). The metabolism from GAP to pyruvate is presented in in Eq. (13).

$$S_{MeOH} \xrightarrow{q_{MeOH}} S_{For} \tag{9}$$

$$S_{For} \xrightarrow{r_S} \frac{1}{3} GAP - ATP \tag{10}$$

$$S_{For} \xrightarrow{\varphi r_S} CO_2 + 2NADH \tag{11}$$

$$S_{For} \xrightarrow{\frac{1}{3}\mu K_{B1}} Cell\ material \tag{12}$$

$$S_{GAP} \xrightarrow{r_{GAP}} pyruvate + 2ATP + NADH \tag{13}$$

The formation of byproducts during the methanol phase was also neglected, since the specific growth rate was controlled relatively low. Therefore, the metabolic pathways after pyruvate and the respiratory chain were assumed to be the same as those in glycerol phase. It should be pointed out that some model parameters, such as K_{B1}, K_{B2} *etc.*, may take dissimilar values depending on different phases.

3.3 Modeling equations

Based on above statement, the structured model for glycerol phase is presented in Eq. (14), which describes the balances of the carbon source, NADH, ATP and pyruvate. These balance relationships are obtained from Eqs. (1)~(3); (2), (4)~(7); (2), (5)~(8); (2), (4), respectively.

$$\begin{bmatrix} 1 & K_{B1} & 0 & 0 \\ 2 & -4K_{B2} & 5 & -2 \\ 1 & -K_{B2} - \dfrac{1}{Y_{ATP}} & 1 & 2P/O \\ 1 & 0 & -1 & 0 \end{bmatrix} \begin{bmatrix} r_S \\ \mu \\ r_{Ac} \\ q_{O2} \end{bmatrix} = \begin{bmatrix} q_{Gly} \\ 0 \\ m_{ATP} \\ 0 \end{bmatrix} \tag{14}$$

The specific glycerol uptake rate q_{Gly} is described with Monod kinetics, see Eq. (15)

$$q_{S,M} = \frac{q_{Glymax} S_{Gly}}{K_{Gly} + S_{Gly}} \tag{15}$$

However, as a common observation in bioprocesses, it was found that the actual glycerol uptake rate was

much lower than $q_{S,M}$ in the early batch stage. Actually, it is known that Monod kinetics covers only the rapid metabolic regulation, but the pathways for gluconeogenesis are subject to long-term regulation by enzyme induction and repression during batch stage (Bellgardt, 1983). An extended first order closed-loop regulator is introduced to describe the lag phase, which was proposed and well validated by Bellgardt, *et al.* (1986). The regulator model is described with Eq. (16). The actual specific glycerol uptake rate q_{Gly} is obtained according to Eq. (17)

$$\frac{dq_{\lim}}{dt} = k_1(q_{Gly} + q_{\lim 0}) + (-k_2 - \mu)q_{\lim} \quad (16)$$

$$q_{Gly} = \begin{cases} q_{S,M} & if\ q_{S,M} < q_{\lim} \\ q_{\lim} & if\ q_{S,M} \geq q_{\lim} \end{cases} \quad (17)$$

In the methanol phase, the balance equations for carbon source, NADH, ATP and pyruvate are obtained from Eqs. (9)~(12); (4)~(7), (11), (13); (5)~(8), (10); (4), (10), (13), respectively, see Eq. (18).

$$\begin{bmatrix} 1+\varphi & \frac{1}{3}K_{B1} & 0 & 0 \\ \frac{1}{3}+2\varphi & -4K_{B2} & 5 & -2 \\ -\frac{1}{3} & -K_{B2}-\frac{1}{Y_{ATP}} & 1 & 2P/O \\ \frac{1}{3} & 0 & -1 & 0 \end{bmatrix} \begin{bmatrix} r_S \\ \mu \\ r_{Ac} \\ q_{O2} \end{bmatrix} = \begin{bmatrix} q_{MeOH} \\ 0 \\ m_{ATP} \\ 0 \end{bmatrix} \quad (18)$$

The specific protein production rate ρ was assumed to follow the model Eq. (19).

$$\rho = a\mu + b \quad (19)$$

3.4 Bioreactor model

The bioreactor model is established based on mass balance. It includes four balance equations for medium volume, biomass, substrate and product concentrations, see Eqs. (20)~(23), where the coefficient of evaporation α was estimated by 0.0006 l (l h)$^{-1}$ based on the mass balance data of the given equipment.

$$\frac{dV_F}{dt} = F_S + F_{NH3} - F_O - \alpha V_F \quad (20)$$

$$\frac{dX}{dt} = \mu X - \frac{F_S + F_{NH3}}{V_F} X + \alpha X \quad (21)$$

$$\frac{dS}{dt} = \frac{F_S}{V_F} S_R - q_S M_S X - \frac{F_S + F_{NH3}}{V_F} S + \alpha S \quad (22)$$

$$\frac{dP}{dt} = \rho X - \frac{F_S + F_{NH3}}{V_F} P + \alpha P \quad (23)$$

The coupling of the structured kinetic model and the bioreactor model is shown in Fig. 1.

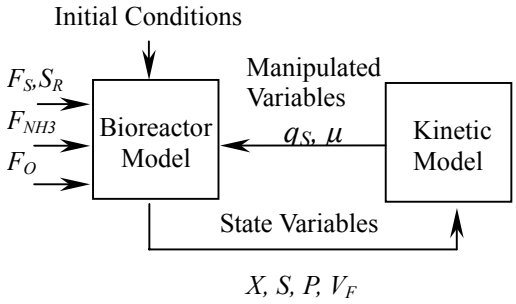

Fig.1 Combined metabolic-bioreactor model

3.5 Validation of the model

Several experiments were carried out to validate the model, and two of them were shown in Fig. 2. It was found that both cell growth and protein production are well described by the model. For confidential reasons, the scale has been removed in this figure as well as in other figures.

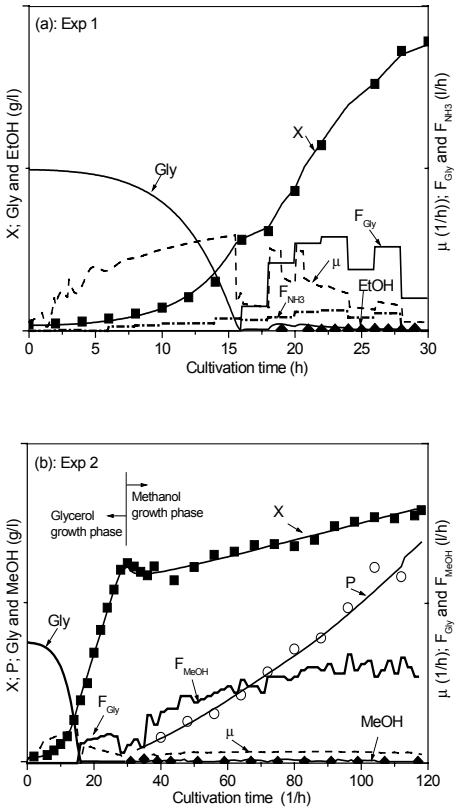

Fig. 2 Comparison of model simulation with measurements. Lines: model simulation; symbols: measurements.

There are seventeen model parameters in Eqs. (14)~(16), (18) and (19). Three of them took fixed values as those for baker's yeast as listed in Table. 1 (Yuan and Bellgardt, 1994). The rest were identified by the Simplex method (Nelder and Mead, 1965), see Tables 2 and 3.

Table 1 Parameters taking fixed values as those for baker's yeast

Para.	Y_{ATP}	P/O	q_{lim0}
Unit	g mol^{-1}	mol mol^{-1}	mol $(gh)^{-1}$
Value	10.5	1.5	0.0006

Table 2 Parameters identified for glycerol growth phase

Para.	q_{Glymax}	K_{Gly}	m_{ATP}	K_{B1}	K_{B2}	k_1	k_2
Unit	mol $(gh)^{-1}$	g l^{-1}	mol $(gh)^{-1}$	mol g^{-1}	mol g^{-1}	h^{-1}	h^{-1}
Exp.1	0.0057	0.05	0.001	0.001	0.014	0.6	0.3
Exp.2	0.0057	0.04	0.001	0.001	0.013	0.5	0.3

Table 3 Parameters identified for methanol growth phase

Para.	$q_{MeOHmax}$	K_{MeOH}	m_{ATP}	K_{B1}	K_{B2}	a	b
Unit	mol $(g)^{-1}$	g l^{-1}	mol $(gh)^{-1}$	mol g^{-1}	mol g^{-1}	-	h^{-1}
Exp.2	0.001	0.16	0.0001	0.015	0.013	0.04	0.0001

4. Model Based Feeding Control

In the literature, exponential type feeding strategy has been proven to be beneficial for improving the recombinant proteins productivity of *Escherichia coli* system (Paalme, *et al*., 1990; Yee and Blanch, 1992). According to the standard protocol, the methanol feeding rate is constant. Such feeding strategy results in a decreasing specific growth rate. This may be one of the reasons for the low productivity of rHSA found in our study (data not shown). Therefore, exponential type methanol feeding profiles are designed with the support of the model. The goal is to maintain the specific growth rate at preset values during the production stage. The sum of squared errors of the specific growth rate between model simulation and the preset value during the whole production stage was chosen as the objective function. First, the increasing type of feeding profile is used during induction stage (30⩽t⩽40h), see Eq. (24). The slope of ω_1 was optimized by Golden Section Search to make the specific growth rate as close as possible to the preset value at 40 h. During production stage (t>40h), the feeding profile shown in Eq. (25) is used. Obviously, the constant ω_2 can be calculated as ($10\omega_1$+12). The parameter ω_3 was then estimated with the same method. Two additional experiments were carried out to validate the control strategy. The results of the control experiments are illustrated in Fig. 3.

$$F(t) = \omega_1 (t - 30) + 12 \qquad 30 \leqslant t \leqslant 40h \qquad (24)$$

$$F(t) = \omega_2 \exp(\omega_3 (t - 40)) \qquad t > 40h \qquad (25)$$

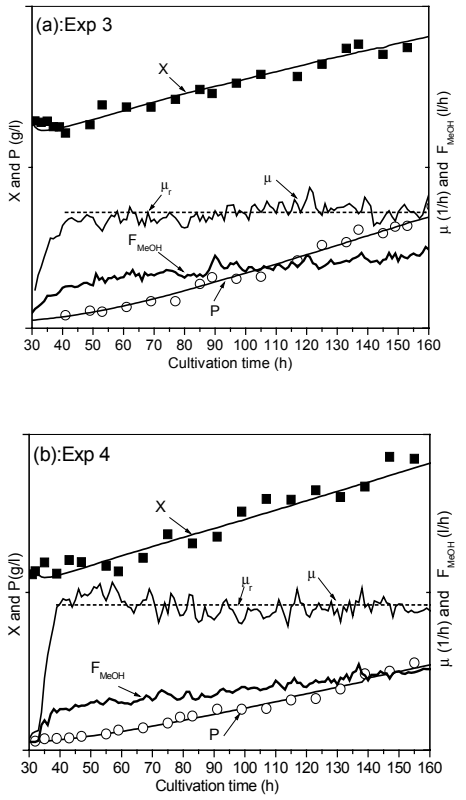

Fig.3 Experiments to test the model based feeding profile. Lines: model simulation; symbols: measurements.

5. Discussion and Conclusion

In this paper, a structured model for *Pichia pastoris* was constructed and validated. Based on the model, the specific growth rate was successfully controlled at predetermined constant levels in the methanol phase. The metabolic model is established based on the simplified flux analysis. It is more complicated in comparison with the mass balance model found in the literature (Kobayashi, *et al*., 2000). However, it enables further investigations on metabolic fluxes. Moreover, this structured model may be applied in those situations, where the set point control of residual methanol concentration is required. It was also found that most model parameters have relative constant values for different experiments, which implies that the model is robust to some extent.

For the methanol phase, Veenhuis, *et al*. (1983) pointed out that the dissimilation of formaldehyde generates the primary part of energy source NADH. That means, the flux of dissimilation plays a significant role in the metabolic network. On the other hand, according to Sibirny *et al*. (1990), the most energy for methanol growth comes from the assimilatory pathway, and the main function of

dissimilation of formaldehyde is to protect the cell from the toxic effect of the accumulated formaldehyde. In this paper, higher flux via assimilatory pathways (corresponding to lower φ) was adopted.

6. Acknowledgements

The authors gratefully acknowledge the support of the North China Pharmaceutical Company, the Natural Science Foundation of China (Grant No. 60174024) and the National High Technology Research and Development Program of China (Grant No. 2001AA413110). Earlier study of this work was supported by the Alexander von Humboldt Foundation/Germany. The comments of Prof. Dr. K.-H. Bellgardt of the Institut fuer Technische Chemie, University Hannover/Germany are also gratefully acknowledged.

7. Nomenclature

EtOH	ethanol residual concentration g l^{-1}
F_S	substrate feeding rate l h^{-1}
F_{Gly}	glycerol feeding rate l h^{-1}
F_{MeOH}	methanol feeding rate l h^{-1}
F_{NH3}	ammonia solution feeding rate l h^{-1}
F_O	withdrawal rate cause by sampling l h^{-1}
Gly	glycerol concentration in the medium g l^{-1}
m_{ATP}	maintenance coefficient for ATP mol (g $h)^{-1}$
MeOH	methanol concentration in the medium g l^{-1}
M_S	molecular weight of substrates
P	heterologous protein concentration g l^{-1}
P/O	effectiveness coefficient of oxidative phosphorylation
q_{Gly}	actual specific uptake rate of glycerol mol (g $h)^{-1}$
q_{lim}	specific uptake rate of glycerol obtained from regulator model mol(g $h)^{-1}$
q_{lim0}	initial value of specific uptake rate of glycerol mol(g $h)^{-1}$
$q_{S,M}$	specific uptake rate of glycerol obtained from Monod model mol(g $h)^{-1}$
q_{MeOH}	specific methanol uptake rate mol(g $h)^{-1}$
q_{O2}	specific oxygen uptake rate mol (g $h)^{-1}$
q_S	specific substrate uptake rate mol (g $h)^{-1}$
r_{Ac}	specific acetyle-CoA production rate mol (g $h)^{-1}$
r_{ATP}	specific ATP uptake rate mol(g $h)^{-1}$
r_{GAP}	specific glyceraldehydes-3-phosphate uptake rate mol(g $h)^{-1}$
r_{NAD}	specific NADH uptake rate in respiratory chain mol(g $h)^{-1}$
r_S	specific rate of glycolysis mol(g $h)^{-1}$
r_{TCA}	specific acetyle-CoA uptake rate mol(g $h)^{-1}$
S	substrate concentration in the medium g l^{-1}
S_{MeOH}	extracellular methanol concentration g l^{-1}
S_R	substrate concentration in the feed g l^{-1}
S_{Gly}	extracellular glycerol concentration g l^{-1}
S_{GP}	intracellular glycerol 3-phosphate concentration g l^{-1}
S_{For}	intracellular formaldehyde concentration g l^{-1}
V_F	volume of broth l
X	biomass concentration g l^{-1}
Y_{ATP}	yield coefficient of ATP g mol^{-1}
α	coefficient of evaporation l (l $h)^{-1}$
μ	specific growth rate h^{-1}
μ_r	preset value of the specific growth rate h^{-1}
ρ	specific product formation rate h^{-1}
φ	ratio of formaldehyde consumed between dissimilatory and assimilatory pathways
Suffix max	maximum values of the corresponding parameters or variables
K_{B1}, K_{B2}, K_{Gly}, K_{MeOH}, *a, b,* k_1, k_2	model parameters

References

Bellgardt, K.-H. (1983). Modellbidung des Wachstums von Saccharomyces cerevisiae in Ruhrkesselreactoren. Ph.D Dissertation, University of Hannover.

Bellgardt, K.-H., W. Kuhlmann, H.D. Meyer, K. Schügerl and M. Thoma (1986). Application of an extended Kalman filter for state estimation of a yeast fermentation. *IEE PROCEEDING*, **133,** 226-234.

Boze, H., L. Celine, C. Patrick, R. Fabien, V. Christine, C. Yves and M. Guy (2001). High-level secretory production of recombinant porcine follicle-stimulating hormone by *Pichia pastoris. PROCESS BIOCHEMISTRY,* **36,** 907-913.

Cereghino, J.L. and J.M. Cregg (2000). Heterologous protein expression in the methylotrophic yeast *Pichia pastoris*. *FEMS Microbiology Reviews*, **24,** 45-66.

Chung, J.D. (2000). Design of Metabolic Feed Controllers: Application to High-Density Fermentation of *Pichia pastoris*. *Biotechnology and Bioengineering*, **68,** 298-307.

d'Anjou, M.C. and A.J. Daugulis (1997). A model-based feeding strategy for fed-batch fermentation of recombinant *Pichia pastoris*. *Biotechnology Techniques*, **11,** 865-868.

Gancedo, G., J.M. Gancedo and A. Sols (1968). Glycerol Metabolism in Yeasts Pathways of Utilization and Production. *European J. Biochem*, **5,** 165-172.

Gellissen, G. (2000). Heterologous protein production in methylotrophic yeast, *Appl Microbiol Biotechnol,* **54,** 741-750.

Jahic, M., J.C. Rotticci-Mulder, M. Martinelle, K. Hult and S.O. Enfors (2002). Modeling of growth and energy metabolism of *Pichia pastoris* producing a fusion protein. *Bioprocess Biosyst Eng.,* **24,** 385-393.

Jimenez, R.E., K. Sanchez, H. Roca and J.M. Delgado (1997). Different methanol feeding strategies to recombinant *Pichia pastoris* cultures producing high level of dextranase, *Biotech. Techniques*, **11,** 461-466.

Kobayashi, K., S. Kuwae, T. Ohya, T. Ohda, M. Ohyama and K. Tomomitsu (2000). High level secretion of recombinant human serum albumin by fed-batch fermentation of methylotrophic yeast, *Pichia pastoris*, Based on Optimal Methanol Feeding Strategy, *Journal Bioscience and Bioengineering*, **90,** 280-288.

Lueers, G.H., R. Advani, T. Wenzel and S. Subramani (1998). The *Pichia pastoris* dihydroxyacetone kinase is a PTS1-containing, but cytosolic, protein that is essential for growth on methanol. *Yeast,* **14,** 759-771.

Nelder, R. and J.A. Mead (1965). A simplex method for function minimization, *Comput. J.,* **7,** 308-313.

Nevoigt, E. and U. Stahl (1997). Osmoregulation and glycerol metabolism in the yeast *Saccharomyces cerevisiae*. *FEMS Microbiology Reviews*., **21,** 231-241.

Paalme, T., K. Tiisma, A. Kahru, K. Vanatalu and R. Vilu (1990). Glucose-limited fed-batch cultivation of *Escherichia coli* with computer-controlled fixed growth rate. *Biotechn. Bioeng.,* **35,** 312-319.

Ratledge, C. and B. Kristiansen (2001). *Basic Biotechnology*, pp. 17-45. Cambridge University Press, England.

Sibirny, A.A., V.M. Ubiyvovk, M.V. Gonchar, V.I. Titorenko, A.Y. Voromovsky, Y.G. Kapultsevich and K.M. Bliznik (1990). Reactions of direct formaldehyde oxidation to CO_2 are non-essential for energy supply of yeast methylotrophic growth. *Arch. Microbiol,* **154,** 566-575.

Sonnleitner, B. and O. Kaeppeli (1986). Growth of *Saccharomyces cerevisiae* is controlled by its limited respiratory capacity: Formation and verification of a hypothesis. *Biotechnol. Bioeng,* **28,** 927-937.

Veenhuis, M., J.P. van Dijken and W. Harder (1983). The significance of peroxisomes in the metabolism of one-carbon compounds in yeasts. *Adv. Microb. Physiol.,* **24,** 1-82.

Yee, L., and H.W. Blanch (1992). Recombinant protein expression in high cell density fed-batch cultures of *Escherichia coli. Bio/Technology*, **10,** 1550-1556.

Yuan, J.Q. and K.-H. Bellgart (1994). Investigations on the optimal control of storage stability of compressed baker's yeast *Saccharomyces cerevisiae*. *Journal of Biotechnology,* **32,** 261-272.

FEEDFORWARD CONTROL OF BATCH CRYSTALLISERS - AN APPROACH BASED ON ORBITAL FLATNESS

Ulrich Vollmer [*] **Jörg Raisch** [*,**]

[*] *Systems and Control Theory Group, Max-Planck-Institut Dynamik komplexer technischer Systeme, 39106 Magdeburg, Germany, Fax: +49-391-6110-518*
[**] *Lehrstuhl für Systemtheorie technischer Prozesse Otto-von-Guericke-Universität 39016 Magdeburg, Germany*

Abstract: This contribution addresses the problem of feedforward control design for batch crystallisers based on moment models. Moment models, which are standard in the crystallisation literature, are shown to be orbitally flat, i.e. they are flat after an appropriate time scaling. The reciprocal of the crystal growth rate serves as the time scaling function such that a new notion of 'time' is defined by the increase in crystal length. For any desired final crystal size distribution (CSD) which is compatible with the crystalliser model it is possible, exploiting flatness, to analytically compute the corresponding temperature trajectory.

Keywords: batch crystallisation, population balance, orbital flatness, process control

1. INTRODUCTION

The quality of crystalline products in the chemical and pharmaceutical industry is not solely determined by their chemical composition but also by physical properties, primarily by the crystal size distribution (CSD). Therefore, the manufacturing of crystalline material with a pre-defined CSD is one of the current challenges in industrial crystallisation (Rawlings *et al.*, 1993). In batch cooling crystallisers, the CSD can be influenced by the cooling strategy, i.e. the temperature-time-profile, applied to the crystalliser.

The temporal evolution of CSD in the domain of time and crystal size can be modelled by a partial differential equation (PDE) referred to as the *population balance equation* (Randolph and Larson, 1988; Ramkrishna, 2000). This PDE is coupled to one or more ordinary differential equations (ODE) for, e.g., concentration and temperature of the liquid phase. Under certain conditions, a finite-dimensional model can be derived from this infinite-dimensional system. The resulting model does not describe the evolution of the entire CSD, but only of a number of its moments.

Based on a population balance model, it is of course possible to determine the final product CSD for a given temperature profile by simulation. The inverse problem, i.e. the design of a feedforward control which produces a desired CSD, is an area of active research. The most common approach is to use optimisation techniques in order to determine a temperature profile that produces a CSD which is optimal with respect to some cost function. (Jones, 1974) applied Pontryagin's maximum principle to obtain an optimal cooling policy. Dynamic optimisation was applied, for example, in (Miller and Rawlings, 1994; Lang *et al.*, 1999; Chung *et al.*, 1999; Zhang and Rohani, 2002).

In this contribution, optimisation techniques are *not* used. Instead the feedforward control problem

for batch cooling crystallisers is solved exploiting *differential flatness* (Fliess *et al.*, 1992; Fliess *et al.*, 1995*b*). The batch crystalliser model can be shown to be flat after an appropriate time scaling. Such systems are called *orbitally flat* (Fliess *et al.*, 1995*a*; Respondek, 1998; Guay, 1999). It is well known that flat systems possess a certain invertibility property and, therefore, trajectory planning and feedforward control design can be done in a very elegant way (Rouchon *et al.*, 1993).

This paper is organised as follows. In the following section, orbital flatness is defined. In Section 3, a population balance model for a batch cooling crystalliser is presented and a moment model for this system is derived. In Section 4, orbital flatness of the moment model is established. Furthermore, it is shown that, based on orbital flatness, a temperature profile can be computed which produces any given final CSD compatible with the model. This is, to the authors' knowledge, the first time this problem has been solved for batch crystallisation.

2. ORBITAL FLATNESS

The notion of flatness can be mathematically defined in a differential algebra setting (Fliess *et al.*, 1995*b*) or in the context of differential geometry of infinite jets and prolongations (Fliess *et al.*, 1999). In this section, a less formal, more intuitive definition of flatness is given (Rothfuß *et al.*, 1996). A finite-dimensional dynamic system

$$\dot{x}(t) = f(x(t), u(t)),\ x(t) \in I\!R^n,\ u(t) \in I\!R^m \quad (1)$$

is called *differentially flat*, or simply *flat*, if there exists a fictitious output $y(t) \in I\!R^m$ which satisfies the following conditions.

A The output $y(t)$ can be expressed as a function of the system state $x(t)$ and input $u(t)$ and finitely many time derivatives of the input

$$y(t) = \Phi\left(x(t), u(t), \dot{u}(t), \dots u^{(\alpha)}(t)\right). \quad (2)$$

B Reversely, the system state and input can be expressed as functions of the output $y(t)$ and finitely many of its time derivatives

$$x(t) = \Psi_1\left(y(t), \dot{y}(t), \dots, y(t)^{(\beta)}\right) \quad (3\text{-a})$$

$$u(t) = \Psi_2\left(y(t), \dot{y}(t), \dots, y(t)^{(\beta+1)}\right) \quad (3\text{-b})$$

The fictitious output $y(t)$ is then called a *flat output*. It completely determines the dynamic behaviour of system (1). If a sufficiently smooth trajectory of the flat output is given, the trajectories of the entire system state $x(t)$ and the system input $u(t)$ are determined by (3-a) and (3-b), respectively. They can be computed without solving a differential equation. Therefore, it is obvious that flatness is a property which facilitates the problems of trajectory planning and design of feedforward control considerably. Since the flat output constitutes an algebraic parameterisation of the system's dynamics, flatness also is a particularly useful property for the solution of dynamic optimisation problems.

Allowing an appropriate state-dependent time scaling, the advantages of flat systems can be extended to a somewhat larger class of systems (Fliess *et al.*, 1995*a*; Respondek, 1998; Guay, 1999). A new 'time'-variable τ is defined as follows:

$$[t_0 \quad t_{end}] \mapsto [\tau_0 \quad \tau_{end}]$$
$$\frac{dt}{d\tau} = s(x(t), u(t)), \quad \tau(t_0) = \tau_0. \quad (4)$$

The mapping of t to τ is bijective iff

$$0 < s(x(t), u(t)) < \infty, \quad \forall t. \quad (5)$$

This makes the time transformation invertible; hence, a control law $u(\tau)$ designed in new time τ can be transformed back and applied in real time t. In new 'time', the system (1) evolves according to

$$\frac{dx}{d\tau} = \underbrace{f(x(\tau), u(\tau))s(x(\tau), u(\tau))}_{=:g(x(\tau), u(\tau))}. \quad (6)$$

If the time scaled system (6) is flat then the original system (1) is called *orbitally flat*.

3. BATCH CRYSTALLISER MODEL

A batch cooling crystalliser (Figure 1) is operated as follows. Initially, the crystalliser contains undersaturated solution. As the solution is cooled, it becomes supersaturated. At this point, small seed crystals may be added. Supersaturation drives the formation of new crystals and the growth of existing crystals. Both processes, nucleation and growth, consume solute from the solution such that the concentration decreases while the amount of crystalline material increases. At the end of the batch the vessel is discharged and the product undergoes further processing steps such as filtering and drying. Product quality as well as the efficiency of downstream processing is heavily influenced by the CSD.

For modelling purposes, the size of crystals is defined by a characteristic length L. A number density function $f(L, t)$ representing the number of crystals per crystal length and volume of slurry formalises the concept of CSD (Randolph and Larson, 1988).

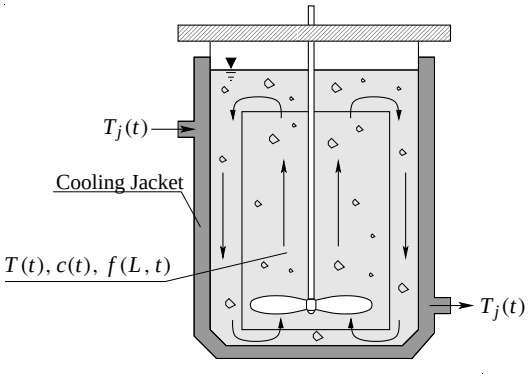

Fig. 1. Sketch of a batch cooling crystalliser

In the following, a standard model for batch crystallisers (Miller and Rawlings, 1994) is presented. It is assumed that all crystals grow at the same rate, i.e. the growth rate G is independent of crystal size, and that nuclei have a negligibly small size. Writing down a balance equation for the number of crystals in an infinitesimal interval of crystal length, a PDE is obtained which, together with appropriate initial and boundary conditions, describes the temporal evolution of the CSD

$$\frac{\partial f(L,t)}{\partial t} = -\frac{G(t)\partial f(L,t)}{\partial L} \tag{7-a}$$

$$f(0,t) = \frac{B(t)}{G(t)} \tag{7-b}$$

$$f(L,0) = f_{seed}(L). \tag{7-c}$$

The nucleation rate is denoted by $B(t)$. The size distribution of seed crystals is $f_{seed}(L)$. Equation (7-a) is called the *population balance*. An ordinary differential equation for the solute concentration $c(t)$ is obtained from the mole balance for the liquid phase

$$\frac{dc(t)}{dt} = -3\rho_c k_v h \int_0^\infty L^2 G(t) f(L,t)\, dL, \tag{8}$$

where ρ_c is the density of crystals, h is a conversion factor (volume of slurry per mass of solvent) and k_v is a volume shape factor defined such that the volume of a crystal with length L is $V_{crystal}(L) = k_v L^3$.

The dependence of (secondary) nucleation and growth rates on supersaturation $S(t)$ and CSD $f(L,t)$ is empirically modelled by

$$G(t) = k_g S(t)^g \tag{9}$$

$$B(t) = k_b S(t)^b k_v \int_0^\infty L^3 f(L,t)\, dL, \tag{10}$$

with supersaturation

$$S(t) = \frac{c(t) - c_{sat}(t)}{c_{sat}(t)}. \tag{11}$$

The saturation concentration c_{sat} is modelled by the empirical relation

$$c_{sat}(t) = A_0 + A_1 T(t) + A_2 T(t)^2. \tag{12}$$

The parameters k_g, k_b, g and b depend on the material to be crystallised, the crystalliser geometry and operating conditions whereas A_0, A_1 and A_2 are solely determined by the combination of solute and solvent substances.

According to (9)-(12), the rates of nucleation $B(t)$ and growth $G(t)$ depend on the temperature $T(t)$. Hence, $T(t)$ can be used as a manipulated variable to affect the CSD. As the temperature $T(t)$ cannot be influenced directly, a subsidiary feedback controller may be used which controls the temperature $T(t)$ by manipulating the cooling jacket temperature $T_j(t)$.

From population balance (7-a) with boundary condition (7-b), a set of ODEs for the moments of the CSD

$$\mu_i(t) := \int_0^\infty L^i f(L,t)\, dL, \quad i = 0, 1, 2, \ldots \tag{13}$$

can be derived. The zeroth moment $\mu_0(t)$ gives the overall number of crystals. The second moment $\mu_2(t)$ is proportional to the overall crystal surface, and the third moment $\mu_3(t)$ is proportional to the volume of the crystalline material in the crystalliser.

Since the duration of the batch, t_{end}, is finite and the growth rate $G(t)$ is bounded it follows that the size of crystals is bounded also. Hence, there is a maximum length L_{max} such that the following is true

$$f(L,t) = 0, \quad \forall L > L_{max}. \tag{14}$$

Consequently, by partial integration it follows from (7-a), (7-b) that

$$\frac{d\mu_0(t)}{dt} = B(t)$$
$$\frac{d\mu_i(t)}{dt} = iG(t)\mu_{i-1}(t), \quad i = 1, 2, \ldots \tag{15}$$

Since the overall mass of solute in the crystalliser is constant, an additional algebraic equation can be derived, relating the third moment $\mu_3(t)$ and the solute concentration $c(t)$

$$c(t) = c_0 + \rho_c k_v h(\mu_{3,Seed} - \mu_3(t)), \tag{16}$$

where c_0 is the initial solute concentration and $\mu_{3,Seed} := \int_0^\infty f_{seed}(L)\, dL$ is the third moment of the seed CSD. Note that the integral expression in (10) is the third moment, i.e. $B(t) = k_b k_v S(t)^b \mu_3(t)$. Because of (9),(11),(12) and (16),

$B(t)$ and $G(t)$ are entirely determined by $\mu_3(t)$ and $T(t)$. Hence, the differential equations for the first four moments can be written as

$$\frac{d\mu_0(t)}{dt} = B(\mu_3(t), T(t)) \quad (17\text{-a})$$
$$\frac{d\mu_1(t)}{dt} = G(\mu_3(t), T(t)) \cdot \mu_0(t) \quad (17\text{-b})$$
$$\frac{d\mu_2(t)}{dt} = 2G(\mu_3(t), T(t)) \cdot \mu_1(t) \quad (17\text{-c})$$
$$\frac{d\mu_3(t)}{dt} = 3G\left(\mu_3(t), T(t)\right) \cdot \mu_2(t), \quad (17\text{-d})$$

This constitutes a simplified model for the batch crystalliser. It is clearly nonlinear, but finite-dimensional. The moments $\mu_0(t) \dots \mu_3(t)$ are the system states, and temperature $T(t)$ serves as the control input. This model exactly describes the dynamics of the moments of the CSD but it does, of course, not describe the evolution of the entire CSD. However, as mentioned above, the moments have a clear physical meaning and for many applications they represent the most important aspects of the CSD.

4. FEEDFORWARD CONTROL

4.1 *Flatness of crystalliser model*

In this paragraph, it is demonstrated that system (17-a)-(17-d) is orbitally flat. With scaling function

$$s(t) = \frac{1}{G(\mu_3(t), T(t))}, \quad (18)$$

a new notion of time is defined by

$$d\tau = G(\mu_3(t), T(t))dt, \quad \tau_0 = 0. \quad (19)$$

As G represents the crystal growth rate, the new 'time' τ is the increase in length which crystals have gained since the beginning of the batch. This is a very natural way to describe the progression of the batch. According to (5), the scaling function has to be strictly positive and finite. Because of (9) and (11), this implies that the liquid in the crystalliser has to be kept supersaturated, i.e. $c(t) > c_{sat}(t)$, $\forall t$. Since in a crystalliser crystals are to be grown rather than dissolved this condition makes eminent sense from a practical point of view. Using new time τ, the system (17-a)-(17-d) is transformed to

$$\frac{d\mu_0(\tau)}{d\tau} = \frac{B(\mu_3(\tau), T(\tau))}{G(\mu_3(\tau), T(\tau))} \quad (20\text{-a})$$
$$\frac{d\mu_1(\tau)}{d\tau} = \mu_0(\tau) \quad (20\text{-b})$$
$$\frac{d\mu_2(\tau)}{d\tau} = 2\mu_1(\tau) \quad (20\text{-c})$$
$$\frac{d\mu_3(\tau)}{d\tau} = 3\mu_2(\tau). \quad (20\text{-d})$$

It is now shown that for the output

$$y(\tau) = \mu_3(\tau) \quad (21)$$

both conditions A and B in the definition of flatness hold. As $\mu_3(\tau)$ is a state variable, (2) and therefore requirement A hold trivially. Differentiating the output $y(\tau)$ four times with respect to τ yields

$$\frac{dy(\tau)}{d\tau} = 3\mu_2(\tau) \quad (22\text{-a})$$
$$\frac{d^2y(\tau)}{d\tau^2} = 6\mu_1(\tau) \quad (22\text{-b})$$
$$\frac{d^3y(\tau)}{d\tau^3} = 6\mu_0(\tau) \quad (22\text{-c})$$
$$\frac{d^4y(\tau)}{d\tau^4} = 6\frac{B(\mu_3(\tau), T(\tau))}{G(\mu_3(\tau), T(\tau))}. \quad (22\text{-d})$$

From (21), (22-a)-(22-c) it is obvious that the states $\mu_3(\tau) \dots \mu_0(\tau)$ can be computed from $y(\tau)$ and its first three derivatives. The input $T(\tau)$ can be determined from (22-d) by additionally using the fourth derivative. Hence, equations (3-a), (3-b) and therefore requirement B also hold. Consequently, $y(\tau)$ is a flat output, and the transformed system (20-a)-(20-d) is flat. This implies orbital flatness of the moment model (17-a)-(17-d) in original time.

4.2 *Control synthesis procedure*

In the following, two characteristics of the batch crystalliser model are exploited to facilitate feedforward control design. These characteristics are, on the one hand, the orbital flatness property of the moment model and, on the other hand, the simple form of the population balance equation (7-a) when rewritten in new time τ. Applying the time scaling (19) to the original PDE (7-a) yields the simple transport equation

$$\frac{\partial f(L,\tau)}{\partial \tau} = -\frac{\partial f(L,\tau)}{\partial L}. \quad (23)$$

This implies that $f(L,t)$ is constant on straight lines in the (L,τ)-domain with $\frac{dL}{d\tau} = 1$, see Figure 2. Furthermore, the size distribution $f(L,\tau)$ can be split into two parts, where one part represents grown seed crystals

$$f_s(L,\tau) = f(L,\tau), \quad \text{for } L \geq \tau \quad (24)$$

and the other part describes the distribution of crystals produced by nucleation

$$f_n(L,\tau) = f(L,\tau), \quad \text{for } L < \tau. \quad (25)$$

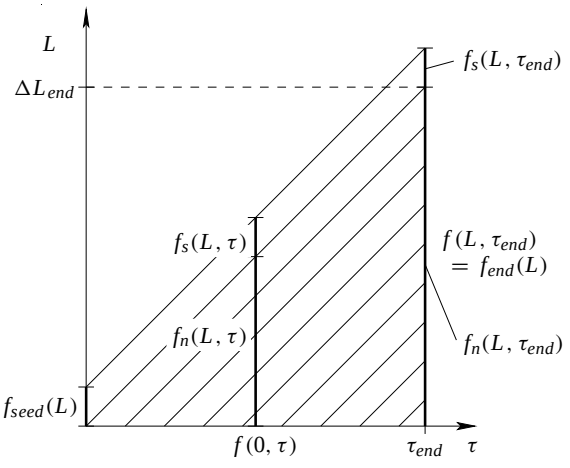

Fig. 2. Evolution of CSD in the (L,τ)-domain

Obviously, the distribution of grown seed crystals $f_s(L,\tau)$ cannot be influenced by control since it is equivalent to the initial seed distribution shifted in size by the length $\Delta L = \tau$, i.e. $f_s(L,\tau) = f_{seed}(L+\tau)$. In contrast, the distribution of particles created by nucleation $f_n(L,\tau)$ can be influenced by appropriate manipulation of the crystalliser temperature $T(\tau)$, since nucleation rate $B(\tau)$ depends on temperature. Consequently, a necessary condition for a desired CSD at the end of the batch $f_{end}(L)$ to be attainable is

$$f_{end}(L) = f_{seed}(L - \Delta L_{end}), \quad \text{for } L \geq \Delta L_{end}, \tag{26}$$

where $\Delta L_{end} = \tau_{end}$ is the increase in size which a crystal gains over the whole batch run.

Since $f(L,\tau)$ is constant on the characteristic lines $\frac{dL}{d\tau} = 1$, the values of a desired $f_{end}(L)$ in the size range $0 \leq L < \Delta L_{end}$ can be traced back to values of the CSD at the lower boundary of the size range $f(0,\tau)$ for $0 < \tau \leq \tau_{end}$. Consequently, if the CSD at the end of the batch is fixed to a certain desired distribution

$$f(L,\tau_{end}) = f_{end}(L), \tag{27}$$

then the time profile of the boundary condition that is necessary to produce the desired distribution $f_{end}(L)$ is determined by

$$f(0,\tau) = f_{end}(\tau_{end} - \tau), \quad 0 < \tau \leq \tau_{end}. \tag{28}$$

Note that τ_{end} is equivalent to the maximum length of nucleated crystals ΔL_{end}, which is also fixed when choosing the desired final CSD $f_{end}(L)$. Because of (28) the desired $f_{end}(L)$ determines the trajectory of the boundary condition (7-b) and according to (22-d) this determines the fourth derivative of the flat output

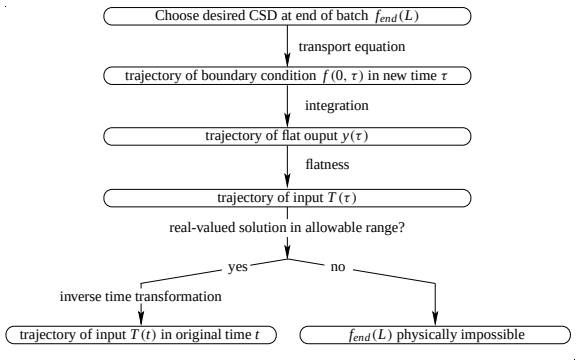

Fig. 3. Open Loop Control Design Procedure

$$\frac{d^4 y(\tau)}{d\tau^4} = 6 f_{end}(\tau_{end} - \tau). \tag{29}$$

The flat output as a function of new time τ is obtained by integrating (29) four times. According to the definition of flatness, all system states and the system input can be determined from the flat output and its derivatives. In particular, the feedforward control $T(\tau)$ which produces the desired final CSD $f_{end}(L)$ can be computed. Eventually, the time transformation (19) has to be inverted to obtain the control $T(t)$ in original time. Depending on the parameterisation of the flat output, the time transformation may not be invertible analytically. Therefore, the inversion may have to be done numerically. In these cases, the open loop control $T(t)$ is determined at a number of time instances but not as an explicit function of time. However, this is not a severe restriction for practical implementation.

Due to the quadratic expression in (12), the solution of (22-d) yields two results for $T(t)$ of which at most one is physically meaningful. If both results are not meaningful, e.g. in the case of complex conjugate solutions, this implies that the desired CSD $f_{end}(L)$ is not compatible with the model, i.e. it cannot be produced by the system from the given initial CSD $f_{seed}(L)$.

Summarising the results of this section, a procedure is obtained which makes it possible to check whether a desired final CSD $f_{end}(L)$ is physically possible and, if so, to compute the corresponding feedforward control $T(t)$. This procedure is depicted schematically in Figure 3. It works as follows. First, a desired CSD $f_{end}(L)$ complying with (26) is chosen. Then, because of the simple structure of the time-transformed population balance, the trajectory of the boundary condition $f(0,\tau)$ in new time is determined by (28). The computation of the flat output $y(\tau)$ basically requires integrating the boundary condition four times. Then, by flatness, the temperature trajectory $T(\tau)$ can be obtained from $y(\tau)$ and its first four derivatives. Finally, the time transformation (19) is inverted

to obtain the feedforward control $T(t)$ in original time.

5. CONCLUSION

It was shown that moment models for batch crystallisation, which are commonly used as a basis for design of feedforward control for these processes, are orbitally flat. The state dependent time scaling function used to render the system flat is physically meaningful: it represents the growth rate of crystals. This leads to a new notion of 'time' which is very natural for the crystallisation process, namely the increase in length of crystals.

The flatness property of the model was exploited for feedforward control design. A procedure was presented to check whether a desired product CSD is achievable and, if so, to *analytically* compute the corresponding control signal, i.e. the temperature trajectory, producing this specific CSD. This is a problem which, so far, has been unsolved in batch crystallisation.

Due to the fact that the flat output completely parameterises the system dynamics, flatness also greatly facilitates the problem of dynamic optimisation of the CSD. Conventionally, the control signal is parameterised, e.g. piecewise linearly. In each optimisation step, the cost function, depending on the final CSD, is determined by numerical solution of the system's differential equations. In a flatness based approach, in contrast, the desired final CSD can be parameterised directly. The corresponding trajectories of system states and input are computed as shown in Section 4 without solving differential equations. Thus, the dynamic optimisation problem is reformulated such that it does not involve the solution of differential equations. This constitutes a significant simplification of this type of problems (Guay *et al.*, 2001). Details on flatness based optimisation of batch crystallisers are presented in (Vollmer and Raisch, 2003).

Furthermore, future work will focus on the extension of the methods presented in this contribution to less restrictive models. In particular, the case of a crystal growth rate that depends on crystal size is of primary interest.

6. REFERENCES

Chung, S.H., D.L. Ma and R.D. Braatz (1999). Optimal seeding in batch crystallization. *Can. J. Chem. Eng.* **77**, 590–596.

Fliess, M., J. Lévine, P. Martin and P. Rouchon (1992). On differentially flat nonlinear systems. In: *Nonlinear Control Systems Design.* pp. 408–412. Pergamon Press.

Fliess, M., J. Lévine, P. Martin and P. Rouchon (1995*a*). Design of trajectory stabilizing feedback for driftless flat systems. In: *Proc. 3rd European Control Conference ECC '95.* pp. 1882–1887.

Fliess, M., J. Lévine, P. Martin and P. Rouchon (1995*b*). Flatness and defect of nonlinear systems: Introductory theory and examples. *Int. J. Contr.* **61**, 1327–1361.

Fliess, M., J. Lévine, P. Martin and P. Rouchon (1999). A Lie-Bäcklund approach to equivalence and flatness of nonlinear systems. *IEEE Trans. Automatic Control* **44**, 922–937.

Guay, M. (1999). An algorithm for orbital feedback linearizaton of single-input control affine systems. *Systems Control Lett.* **38**, 271–281.

Guay, M., S. Kansal and J.F. Forbes (2001). Trajectory optimization for flat dynamic systems. *Ind. Eng. Chem. Res.* **40**(9), 2089–2102.

Jones, A.G. (1974). Optimal operation of a batch cooling crystallizer. *Chem. Eng. Sci.* **29**, 1075–1087.

Lang, Y., A.M. Cervantes and L.T. Biegler (1999). Dynamic optimization of a batch cooling crystallization process. *Ind. Eng. Chem. Res.* **38**, 1469–1477.

Miller, S.M. and J.B. Rawlings (1994). Model identification and control strategies for batch cooling crystallizers. *AIChE Journal* **40**(8), 1312–1327.

Ramkrishna, D. (2000). *Population balances: theory and applications to particulate systems in engineering.* Academic Press.

Randolph, A.D. and M.A. Larson (1988). *Theory of Particulate Processes.* Academic Press, Inc.

Rawlings, J.B., S.M. Miller and W.R. Witkowski (1993). Model identification and control of solution crystallization processes: A review. *Ind. Eng. Chem. Res.* **32**, 1275–1296.

Respondek, W. (1998). Orbital feedback linearization of single-input nonlinear control systems. In: *Proc. of IFAC NOLCOS'98.* Enschede, The Netherlands. pp. 499–504.

Rothfuß, R., J. Rudolph and M. Zeitz (1996). Flatness based control of a nonlinear chemical reactor model. *Automatica* **32**(10), 1433–1439.

Rouchon, P., M. Fliess, J. Lévine and P. Martin (1993). Flatness and motion planning: the car with n trailers. In: *Proc. 2nd European Control Conference ECC '93.* pp. 1518–1522.

Vollmer, U. and J. Raisch (2003). Control of batch cooling crystallisers based on orbital flatness. *Int. J. Contr.* submitted.

Zhang, G.P. and S. Rohani (2002). On-line optimal control of a seeded batch crystallizer. *Chem. Eng. Sci.* in press.